Neurobiology of Disease

Neuronal Loss of *Drosophila* NPC1a Causes Cholesterol Aggregation and Age-Progressive Neurodegeneration

Scott E. Phillips,* E. A. Woodruff III,* Ping Liang, Meaghan Patten, and Kendal Broadie
Department of Biological Sciences, Vanderbilt Kennedy Center for Research on Human Development, Vanderbilt University, Nashville, Tennessee 37232

The mistrafficking and consequent cytoplasmic accumulation of cholesterol and sphingolipids is linked to multiple neurodegenerative diseases. One class of disease, the sphingolipid storage diseases, includes Niemann-Pick disease type C (NPC), caused predominantly (95%) by mutation of the *NPC1* gene. A disease model has been established through mutation of *Drosophila* NPC1a (*dnpc1a*). Null mutants display early lethality attributable to loss of cholesterol-dependent ecdysone steroid hormone production. Null mutants rescued to adults by restoring ecdysone production mimic human NPC patients with progressive motor defects and reduced life spans. Analysis of *dnpc1a* null brains shows elevated overall cholesterol levels and progressive accumulation of filipin-positive cholesterol aggregates within brain and retina, as well as isolated cultured brain neurons. Ultrastructural imaging of *dnpc1a* mutant brains reveals age-progressive accumulation of striking multilamellar and multivesicular organelles, preceding the onset of neurodegeneration. Consistently, electroretinogram recordings show age-progressive loss of phototransduction and photoreceptor synaptic transmission. Early lethality, movement impairments, neuronal cholesterol deposits, accumulation of multilamellar bodies, and age-dependent neurodegeneration are all rescued by targeted neuronal expression of a wild-type *dnpc1a* transgene. Interestingly, targeted expression of *dnpc1a* in glia also provides limited rescue of adult lethality. Generation of *dnpc1a* null mutant neuron clones in the brain reveals cell-autonomous requirements for dNPC1a in cholesterol and membrane trafficking. These data demonstrate a requirement for dNPC1a in the maintenance of neuronal function and viability and show that loss of dNPC1a in neurons mimics the human neurodegenerative condition.

Key words: **Niemann-Pick type C; NPC; lipid storage disease; sphingolipid; endosome; multilamellar body; MLB; visual system; phototransduction**

Introduction

Niemann-Pick type C (NPC), an autosomal-recessive, fatal neurodegenerative disease that typically manifests in childhood (Vanier and Millat, 2003), is classified as a sphingolipid storage disease based on intracellular accumulation of cholesterol, glycosphingolipids, and lyso-bisphosphatidic acid in endosome/lysosome-like organelles (Zervas et al., 2001; Vance, 2006). Lipid accumulation occurs in neurons of the cerebral cortex, cerebellum, and hippocampus (Paul et al., 2004) and in non-neuronal tissues such as liver (Beltroy et al., 2005). Although lipid mistrafficking is the pathological hallmark of NPC, it is unknown whether lipid accumulation is the cause of neurodegeneration or merely an associated consequence of cellular dysfunction.

Received Dec. 14, 2007; revised May 13, 2008; accepted May 15, 2008.

This work was supported by National Institutes of Health Grant NS41740 (K.B.) and National Research Service Award Postdoctoral Fellowship F32 NS058169 (S.E.P.). We are indebted to Drs. Matt Scott and Leo Pallanck for essential *Drosophila* stocks and to the Developmental Studies Hybridoma Bank, University of Iowa, for essential antibodies. We are especially grateful to Drs. David Hachey and Wade Calcutt of the Vanderbilt Mass Spectrometry Core Facility for expert help and use of equipment. We thank Sean Schaffer of the Vanderbilt Cell Imaging Shared Resource Core for assistance and use of equipment. We thank Dr. Larry Zwiebel for the use of his Olympus microscope and Olympus DP70 camera.

*S.E.P. and E.A.W. contributed equally to this work.

Correspondence should be addressed to Prof. Kendal Broadie, 6270 MRB III, 465 21st Avenue South, Nashville, TN 37232. E-mail: kendal.broadie@vanderbilt.edu.

DOI:10.1523/JNEUROSCI.5529-07.2008

 0270-6474/08/286569-14$15.00/0

The vast majority of disease cases (95%) arise from mutations of *NPC1*, with the remainder caused by mutation of *NPC2* (Carstea et al., 1997; Naureckiene et al., 2000). NPC1 is a multipass transmembrane protein that resides in endosome/lysosome-like organelles (Garver et al., 2000; Scott et al., 2004), with homology to the sterol-sensing regions of SCAP (SREBP cleavage-activating protein) and HMG-CoA (3-hydroxy-3-methylglutaryl coenzyme A), proteins involved in cholesterol homeostasis (Davies and Ioannou, 2000; Millard et al., 2005). Recent data suggest that NPC1 directly binds cholesterol and oxysterols *in vitro* (Ohgami et al., 2004; Infante et al., 2007). NPC2 is a small intralysosomal protein that also binds cholesterol (Friedland et al., 2003). The similar organelle localization of NPC1 and NPC2, and the similar lipid accumulations within these organelles in the absence of either protein, suggests they cooperate in the same lipid trafficking pathway. Nevertheless, the molecular functions of NPC1 and NPC2 remain unknown, including how the loss of either protein leads to progressive neurodegeneration.

The *Drosophila* genome encodes more NPC genes: two NPC1 genes (*dnpc1a* and *dnpc1b*) and eight NPC2 genes. The *dnpc1b* homolog is specifically required in midgut epithelia for the uptake of dietary cholesterol, a role performed by the NPC1-like 1 protein in mammals (Voght et al., 2007). A recent study showed that deleting two *dnpc2* genes causes early death and neurodegen-

eration (Huang et al., 2007). The *dnpc1a* gene is widely expressed and required generally for sterol homeostasis, and specifically for sterol-dependent synthesis of the molting hormone ecdysone (Huang et al., 2005; Fluegel et al., 2006). Early lethality caused by loss of dNPC1a is suppressed by feeding mutants excess levels of ecdysone precursors. Strikingly, no neurodegenerative phenotype has been described in *dnpc1a* mutants, and the role of dNPC1a in neuronal function and viability remains totally uncharacterized.

We report here that neuronal dNPC1a function is required for maintenance of neuronal function and viability. Ultrastructural analyses reveal massive, age-progressive accumulation of multilamellar (MLB) and multivesicular (MVB) bodies in neurons, concurrently with accumulation of cholesterol aggregates. Null *dnpc1a* mutants display age-progressive, nonapoptotic neuron loss in both central brain and retina. Electrophysiology recordings show age-dependent loss of phototransduction currents and loss of photoreceptor synaptic transmission. Targeted neuronal expression of a wild-type *dnpc1a* transgene rescues all these defects. These studies demonstrate that *Drosophila* is a viable model system to study the mechanisms of cholesterol trafficking dysfunction and neurodegeneration caused by loss of NPC1.

Materials and Methods

Drosophila *stocks.* All stocks were grown on standard corn meal/molasses diet at 25°C. A stock of 7-dehydrocholesterol (30 mg/ml) in ethanol was added to 500 ml of medium and mixed thoroughly to ensure adequate dispersion of the sterol. 7-Dehydrocholesterol-supplemented food was made to a final concentration of 0.14 mg/g. The control genotype used in all experiments was w^{1118}. The $dnpc1a^{1}$ null allele and yellow fluorescent protein (YFP)-tagged wild-type *dnpc1a* transgene stock (*UAS-dnpc1a-YFP*) were kindly provided by Dr. M. Scott (Stanford University, Stanford, CA) (Huang et al., 2005). The $dnpc1a^{57A}$ null allele and ring gland *2–286* GAL4 driver stock were kindly provided by Dr. L. Pallanck (University of Washington, Seattle, WA) (Fluegel et al., 2006). The following GAL4 drivers were also used in this study: brain mushroom body (MB) OK107-GAL4 (Connolly et al., 1996), pan-neuronal *elav*-GAL4 (Yao and White, 1994), and glial-specific *repo*-GAL4 (Sepp et al., 2001). A transgenic UAS double-strand RNA interference (RNAi) transgenic line specific for *dnpc1a* (UAS-*dnpc1a* RNAi) was generated for this study. Briefly, the sense fragment was generated by amplifying the last 787 bp of exon 10 and intron 10 and subsequently cloned into pUAST with *Eco*RI and *Not*I restriction sites. The antisense fragment was generated from the same 787 bp construct by PCR with *Not*I and *Xba*I flanked primers. The pUAST-dNPC1a RNAi plasmid was injected into w^{1118} embryos with helper plasmid Δ2–3 to generate multiple lines. The *elav*-GAL4;UAS-*dnpc1a*-RNAi line was produced by standard genetic methods.

Life-span analysis. Life spans were determined by collecting newly eclosed animals and placing them at low density (<20 animals per vial) at 25°C in a constant 12 h light/dark cycle in a humidity-controlled incubator. The aging animals were transferred to new vials at least three times per week, with deaths scored. The life-span plots were generated by calculating the percentage of survivorship every second day and plotting viability as a function of time (days). Animals removed for histological/ultrastructural/electrophysiological analyses were subtracted from total population numbers. The viability comparisons between genotypes used time in days to 50% survival of the population.

Cholesterol measurements. The Amplex Red cholesterol assay kit (Invitrogen) was used to measure both free cholesterol and cholesterol ester levels. Control and mutant animals were raised on food supplemented with 7-dehydrocholesterol through larval development, until puparium formation, and then switched to regular food. Heads were isolated from adult animals 5 d after eclosion. Heads were homogenized in 150 mM NaCl, 50 mM Tris, pH 7.5, and 2 mM EGTA (Fluegel et al., 2006) followed by centrifugation at 5000 rpm for 5 min. The supernatant was then diluted to a final concentration of 100 μg/μl and used to assay total cholesterol concentration per manufacturer instructions. To separately measure free cholesterol and not cholesterol esters, assays were performed without cholesterol esterase. Fluorescence was measured with a Flexstation II (Molecular Devices) and a 530/590 nm filter set.

Mass spectrophotometry. Isolated brains were dissected from control and mutant animals at 5 d after eclosion. Sterols from dissected brains were prepared by Bligh and Dyer extraction (Bligh and Dyer, 1959). Sterols were sulfated and prepared for liquid chromatography tandem mass spectrometry (MS/MS) following Rietveld et al. (1999). Briefly, a [3,4-$^{13}C_2$] cholesterol standard was added to samples, followed by extraction in 1,4-dioxane and sulfation with sulfur trioxide-pyridine complex in absolute pyridine to dried lipid samples. Sample analyses were performed using a Surveyor HPLC system (Thermo Electron), with online degasser, quaternary pump, refrigerated autosampler, and column heater. Tandem mass spectrometric detection was performed using a TSQ Quantum triple-stage quadrupole mass spectrometer (Thermo Electron) equipped with a standard API-1 electrospray source and a 100 μm inner diameter deactivated fused silica capillary. A Zorbax SB-Phenyl column (2.1 mm × 15 cm; MAC-MOD Analytical) was used for all chromatographic separations. The autosampler tray temperatures were maintained at 4°C. Mobile phases were made up of 20 mM ammonium formate in (A) CH_3CN:iPrOH:H_2O (4:1:95) and in (B) CH_3CN:iPrOH:H_2O (50:45:5). Gradient conditions were as follows: 0–1 min, B = 30%; 1–7 min, B = 30–85%; 7–9.5 min, B = 85–30%; 9.5–15 min, B = 30%. The flow rate was maintained at 400 μl. A software-controlled divert valve was used to transfer elutent from 0 to 3 min of each chromatographic run to waste. The total chromatographic run time was 15 min.

Brain filipin cholesterol staining. For *in situ* filipin staining, staged brains from controls and mutants were dissected and fixed for 15 min in 4% paraformaldehyde in 4% sucrose/phosphate buffered sucrose (PBS), followed by washes in PBS (three times for 10 min). A fresh stock solution of filipin (1 mg/ml in DMSO; Sigma-Aldrich) was diluted to a final concentration of 50 μg/ml in PBS (Fluegel et al., 2006). Tissues were incubated in the dark for 30 min at room temperature and rinsed with PBS three times. Tissues were mounted in Vectashield (Vector Laboratories) and immediately visualized with an Olympus FV1000 confocal scanning microscope equipped with a UV laser.

Primary neuronal culture. Primary brain neuron cultures were prepared as described previously (Jiang et al., 2005). Briefly, staged control and mutant animals, 72 h after pupariation, were rinsed with ethanol and autoclaved water two times. Dissected brains were dissociated with enzyme solution [containing 50 U/ml papain activated by L-cysteine (1.32 mM) in dissecting saline (DS; in mM: 137 NaCl, 5.4 KCl, 0.17 NaH_2PO_4, 0.22 KH_2PO_4, 33.3 glucose, 43.8 sucrose, and 9.9 HEPES, pH 7.4)] for 15 min at room temperature. Tissue was washed three times with DS and three times with culturing medium (Ham's F-12/DMEM supplemented with 100 μM putrescine, 30 nM sodium selenite, 20 ng/ml progesterone, 50 μg/ml insulin, 100 μg/ml transferring, and 1 μg/ml 20-hydroxyecdysone) followed by mechanical dissociation and plating onto glass-bottom 35 mm dishes (MatTek) coated with Con A and laminin. Dissociated neurons were maintained in a 23°C humidified 5% CO_2 incubator. After 24 h and every fifth day, conditioned Neurobasal medium [Neurobasal medium plus B27 supplements (Invitrogen) conditioned by non-neuronal mouse brain feeder cell cultures] was added to cultured neurons. Live primary culture neurons were incubated with freshly prepared filipin (50 μg/ml in DMSO or ethanol) and imaged with an Olympus FV1000 confocal scanning microscope.

Brain histology. Control and mutant animals were aged as indicated, and heads were isolated and fixed for 48 h in 4% glutaraldehyde, pH 7.4, at 4°C. Heads were postfixed at room temperature in 1% OsO_4 for 2 h and dehydrated in a standard EtOH series. Heads were put through a transition solvent of propylene oxide for 30 min, placed in propylene oxide/resin for 30 min, and infiltrated with pure resin ERL 4221 [Spurr-mixture; electron microscopy sciences (EMS) grade] overnight at 60°C. Heads were oriented so that the knife blade contacted the posterior end first. Fifteen semithick serial sections (1.0 μm) were cut every 20 μm, collected on glass plates, stained with 0.5% toluidine blue on a hot plate for 1 min, and rinsed with water. Sections were dried on the hot plate before mounting with Permount (EMS grade; VWR) (Finley et al., 2003)

and a coverslip. Light microscopy was done with an Olympus BX60 microscope equipped with an Olympus DP70 1.2.1.108 camera.

Electron microscopy. Isolated heads from staged control and mutant animals were prepared for transmission electron microscopy using standard protocols (Huang et al., 2004). Briefly, heads were fixed in 4% glutaraldehyde at 4°C for 48 h. Samples were then washed in two 10 min changes of PBS and transferred to 1% OsO_4 in PBS for 2 h. Heads were then rinsed with double-distilled water, dehydrated through a series of graded alcohols (30–100%), passed through propylene oxide for 30 min, as a transition solvent before being place in a 50%/50% solution of propylene oxide/spur-mixture for 30 min, followed by pure resin, and left overnight at 60°C to polymerize. The next day, ultrathin sections (50–60 nm) were cut on a Leica Ultracut UCT 54 Ultramicrotome and collected on Synaptek 2x1 mm gold slot notch grids (EMS). Grids were stained on a drop of uranyl acetate for 25 min and a drop of lead citrate for 5 min. Sections were examined on a Phillips CM10 transmission electron microscope, 100 keV equipped with a side-mounted, high-resolution 2-mega pixel CCD camera. Digital images were taken of cross sections of the entire head, which contained both retina and brain. The EM ultrastructural images in Figure 5 are the very next 50–60 nm sections after the toluidine blue sections in Figure 4.

Terminal deoxynucleotidyl transferase-mediated biotinylated UTP nick end labeling assays. Newly eclosed animals were collected and aged for 5 d (w^{1118} control, $n = 6$; *dnpc1a*^{1}, $n = 6$) or 45 d (w^{1118} control, $n = 10$; *dnpc1a*^{1}, $n = 10$). Brains were dissected in PBS, fixed for 15 min in 4% paraformaldehyde, and washed three times in PBS. All terminal deoxynucleotidyl transferase-mediated biotinylated UTP nick end labeling (TUNEL) assays were performed by following the instructions from the *in situ* cell death detection kit (Roche Diagnostics). Briefly, control brains were treated with DNase I (100 U/ml in 50 mM Tris-HCl, pH 7.5, and 1 mg/ml BSA) for 10 min at 25°C. TUNEL reaction mixture (50–100 μl) was added to each sample and incubated for 60 min at 37°C. Images were acquired on a Zeiss Axioskop II plus microscope equipped with a Nikon DS-5mC camera and NIS elements BR 2.3 software.

Mosaic Analysis of Repressible Cell Marker neuronal clonal analysis. The Mosaic Analysis of Repressible Cell Marker (MARCM) clonal technique was used as first described by Lee and Luo (1999). The following MARCM lines were generated by standard genetic methods: (1) *heatshock-FLP*, *mouse CD8-GFP;FRT40A,P-GAL80/CyO;GAL4-OK107*; (2) *y,w;FRT40A/CyO*; (3) *FRT40A,dnpc1a*^{57A}*/CyO*; (4) *FRT40A,dnpc1a*^{1}*/CyO*; and (5) *heatshock-FLP*, *mouse CD8-GFP,elav*^{C155}*-GAL4;FRT40A,P-GAL80/CyO*. Large MARCM clones (hundreds of neurons) were made within the brain MB. Single-neuron MARCM clones were made within the three MB neuron populations of α/β, α′/β′, and γ neurons. Staged embryos were collected within a 4 h window and cultured at 25°C. Mature embryos at 20 h were heat shocked at 37°C for 1 h to induce recombination and clone formation. Animals were then cultured to maturity at 25°C. Multiple MARCM clones in the central brain and retina were made with the pan-neuronal *elav*-GAL4 driver. As above, staged embryos were collected from a 4 h window at 25°C, and embryos were heat shocked at 37°C for 1–3 h at various time points (6, 24, 36, 48, and 72 h). Brains were dissected out at staged intervals in days after adult eclosion. Brains were dissected in 1× PBS, fixed in 4% paraformaldehyde for 30 min, and processed with immunostaining. MB axon lobes were labeled by mouse anti-*Drosophila* Fasciclin II 1D4 (1:20; Developmental Studies Hybridoma Bank, University of Iowa), and MARCM clones were labeled by rat anti-mouse CD8 (1:100; Invitrogen). Primary antibodies were visualized using Cy3-conjugated goat anti-mouse IgG (1:100; Jackson ImmunoResearch) and FITC-conjugated goat anti-rat IgG (1:100; Jackson ImmunoResearch). Clones were compared based on three-dimensional projections from complete Z-stacks from confocal microscopy using a Zeiss 510-meta laser-scanning microscope or the Olympus FV1000 confocal scanning microscope.

Electroretinogram recordings. Staged control and mutant animals were anesthetized for 5 min on ice and immobilized by embedding in dental wax. A reference glass electrode filled with 3 M KCl was inserted into the back of the head. A recording glass microelectrode filled with 3 M KCl was inserted into the center of the retina. All animals were dark adapted for 5 min before recording. Light stimulation (luxeon III, wave length, 470 nm; Lumileds) was provided as 2 s light flashes followed by 18 s of dark. All electroretinogram (ERG) recordings were done at room temperature. Data were captured with Axioscope 9.0 software and analyzed with pClamp 9.0 (Molecular Devices) (Huang et al., 2004).

Statistics. All statistical analyses were done with Microsoft Excel software. Significance levels in figures were represented as $0.05 > p > 0.01$ (*), $0.01 > p > 0.001$(**), and $p < 0.001$(***). All error bars represent SEM, as appropriate for comparison of the mean of means distributions.

Results

Targeted neuronal expression of dNPC1a rescues life span of *dnpc1a* null mutant

Previous reports show that absence of dNPC1a function causes lethality early in larval development because of loss of the cholesterol-based steroid hormone ecdysone; however, this early requirement can be circumvented by supplementing the diet with excess levels of ecdysone precursors during larval development (Huang et al., 2005; Fluegel et al., 2006). Similarly, GAL4-targeted expression of a wild-type *dnpc1a* transgene to the ring gland, the site of ecdysone synthesis, rescues *dnpc1a* null mutants to adulthood. To study the requirements of dNPC1a in the adult nervous system, we used these two techniques to produce adult *dnpc1a* null mutants that were then analyzed in age-progressive studies.

Null *dnpc1a* mutants fed a diet supplemented with 7-dehydrocholesterol (0.14 mg/g) develop through larval stages, pupate, and eclose as anatomically normal adult animals. Nearly all of these null mutants display normal motor coordination, locomotion, and movement behaviors immediately after eclosion. However, with age, mutants develop obvious locomotory defects, evidenced first as a loss of motor coordination and then as progressive defects in movement behaviors. The onset and progression of these defects varies markedly between individuals. To display this variation, Figure 1*A* shows the phenotypes of 20 individual *dnpc1a* null mutant animals placed individually into tubes immediately after eclosion and observed at regular intervals for coordination and locomotion behaviors. Within 48 h after eclosion, >50% of mutant animals appeared sluggish, with reduced movement and limited attempts at climbing or evading tactile contact. Within 72 h, most of these animals show a progressive loss of movement abilities, until movement ceased entirely and the animals died (Fig. 1*A*). Nevertheless, a subset of mutant animals remained normal and active throughout an 8 d period of observation and only later died a premature, early-onset death. These phenotypes mimic the symptoms of human NPC patients with progressive locomotion defects and reduced life spans.

Null *dnpc1a* mutant animals maintained in larger populations appear to survive better than isolated individuals, but nevertheless clearly display the same progressive loss of movement behavior and early-onset lethality (Fig. 1*B*). Genetic background control animal populations (w^{1118}) show essentially no lethality for the first month and then the slow onset of lethality in the second month, with 50% of the population dead at 62 d (Fig. 1*B*, filled triangles). In contrast, null *dnpc1a* mutants display a precipitous and continual lethality starting soon after eclosion, with 50% of the population dead at 28 d (Fig. 1B, filled squares). Severe locomotor defects suggest that the cause of early lethality reflects a neuronal requirement for dNPC1a function. To test this hypothesis, a UAS-driven wild-type *dnpc1a* transgene tagged with YFP (*UAS-dnpc1a-YFP*) was targeted only to neurons with the pan-neuronal *elav*-GAL4 driver (Yao and White, 1994). Neuronal expression of the *dnpc1a* transgene in *dnpc1a* null mutants provides no rescue of the ecdysone-dependent larval lethality

A

Id	Day 1	Day 2	Day 3	Day 4	Day 8
A	+++	+	---		
B	+++	+++	+++	+++	+++
C	+++	+++	+++	+++	---
D	+++	+	---		
E	+++	+/-	---		
F	+++	+/-	---		
G	+++	+/-	---		
H	+++	+	---		
I	+++	+	---		
J	+++	+++	+++	+++	---
K	+++	+++	+++	+++	+++
L	+++	+	---		
M	+++	+	---		
N	+++	+	---		
O	+++	+	---		
P	+++	+	+/-	---	
Q	+++	+++	+	+/-	---
R	+++	+++	+++	+++	+++
S	+++	+++	+++	+++	+++
T	+++	+++	+++	+++	+

B

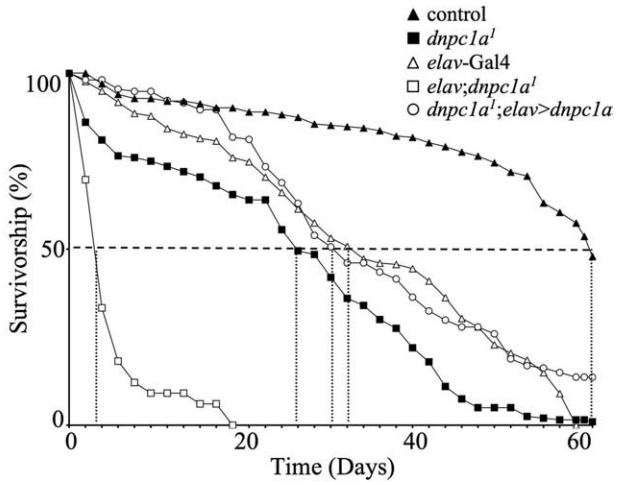

Figure 1. Neural requirement for dNPC1a in age-progressive maintenance of motor behavior and life span. ***A***, Individual "cholesterol-rescued" *dnpc1a* null mutant animals (*dnpc1a*^{1}; $n =$ 20 individual animals) monitored for movement behavior and activity level in days after adult eclosion. The behavioral scale is as follows: +++, normal locomotory activity; ++, reduced activity but normal motor coordination; +, sluggish with reduced coordination; +/−, almost no movement and severely uncoordinated; −, no movement. Id, Identification. ***B***, Adult survival as a function of age determined for the *w*^{1118} genetic control ($n = 231$; filled triangles), *dnpc1a* null mutant (*dnpc1a*^{1}; $n = 124$; filled squares), *elav*-GAL4/+ or *elav*-GAL4/Y;*dnpc1a*^{1}; *UAS-npc1a-YFP*/+ transgenic animals (*dnpc1a*^{1}; *elav*>*dnpc1a*; $n = 73$; open circles), homozygous *elav*-GAL4 or *elav*-GAL4/Y genetic control ($n = 122$; open triangles), and *dnpc1a* null mutants in the homozygous *elav*-GAL4 or elav-GAL4/Y background ($n = 30$; open squares). The age of 50% survivorship (dotted line perpendicular to dashed line at 50%) is 62 d (*w*^{1118}), 28 d (*dnpc1a*^{1}), 33 d (*dnpc1a*^{1};*elav*>*dnpc1a* rescue), 34 d (*elav*-GAL4), and 4 d (*elav*;*dnpc1a*^{1}).

(Huang et al., 2005). However, in cholesterol-rescued adult mutants (*elav*-GAL4/+;*dnpc1a*^{1};*UAS-dnpc1a-YFP*/+), the targeted neuronal expression of dNPC1a strongly rescues the progressive movement defects and the early lethality, extending the life span of *dnpc1a* mutant animals to a comparable age as homozygous *elav*-GAL4 controls (Fig. 1*B*, open circles and open triangles, respectively). Specifically, 50% of *dnpc1a* null animals with targeted neuronal expression live to day 33, compared with day 34 survival for *elav*-GAL4 controls, whereas *dnpc1a* null mutants in the homozygous *elav*-GAL4 background rarely survive past day 10, with 50% lethality by day 4 after eclosion (Fig. 1*B*, open squares). These data demonstrate a specific neuronal requirement for dNPC1a in the maintenance of movement behavior and continued viability with age progression.

Glial astrocyte dysfunction has been linked to neurodegenerative processes caused by NPC1 mutations in mammals (German et al., 2002). The *Drosophila* brain has a dense population of glial cells that are functionally very similar to mammalian glial cells (Freeman and Doherty, 2006). To determine whether dNPC1a function in glial cells can also significantly rescue the early-onset lethality of *dnpc1a* mutant animals, the *repo*-GAL4 driver was used to target expression of the *UAS-dnpc1a-YFP* transgene to glial cells (supplemental Fig. 1, available at www.jneurosci.org as supplemental material) (Sepp et al., 2001). Like the targeted neuronal expression of *dnpc1a*, glial expression of the *dnpc1a* transgene in *dnpc1a* null mutants does not rescue the ecdysone-dependent lethality in larval stages. Similar to the *elav*-GAL4 background, the *repo*-GAL4 background also severely reduces the life span of *dnpc1a* null mutants, with 50% of the population dead by day 4 after eclosion (supplemental Fig. 1, available at www.jneurosci.org as supplemental material). Importantly, targeted glial expression of dNPC1a extends the life span of *dnpc1a* mutant animals, with 50% of the population dead by day 19 (supplemental Fig. 1, available at www.jneurosci.org as supplemental material). However, the *repo*-GAL4 genetic controls live much longer, with 50% of the population dead by day 50 (supplemental Fig. 1, available at www.jneurosci.org as supplemental material). Thus, targeted glial expression of dNPC1a extends the life span of *dnpc1a* null animals (50% lethality by day 19 compared with day 5, respectively); however the life span remains significantly reduced compared with *repo*-GAL4 control animals. Conversely, targeted neuronal expression of dNPC1a in otherwise *dnpc1a* null animals extends the life span to that of *elav*-GAL4 genetic controls (Fig. 1*B*).

Elevated cholesterol levels in *dnpc1a* mutant brains

An age-dependent increase in cholesterol levels in NPC disease is seen in every tissue, except the brain (Xie et al., 1999). In fact, in the homozygous NPC$^{-/-}$ mouse, the concentration of cholesterol in the brain actually decreases with age (Xie et al., 1999). However, the myelin sheaths wrapping neuronal processes are particularly cholesterol rich, and the loss of myelin attributable to neurodegeneration most likely accounts for the overall decrease in brain cholesterol levels in NPC$^{-/-}$ mice, thereby potentially masking cholesterol accumulation within brain neurons. Indeed, at birth, when there is little myelin present, cholesterol levels are elevated in every region of the brain in NPC$^{-/-}$ mice (Xie et al., 2000). *Drosophila* glial cells do not generate myelin sheaths, and there are no known orthologs for the myelin genes (Freeman and Doherty, 2006). Therefore, the *Drosophila* system is well suited to study changes in neuronal cholesterol levels without the influence of cholesterol-rich myelin.

To determine whether cholesterol levels are altered in the brain of *dnpc1a* null mutants, adult heads from control and *dnpc1a* null mutant animals were homogenized, and total cholesterol content was measured by enzymatic assays (Fig. 2). Cholesterol levels in the absence of dNPC1a function are clearly and consistently elevated compared with wild type. The quantified total cholesterol levels in *dnpc1a* mutant heads are more than threefold higher compared with age-matched control animals (*w*^{1118} control, 1.5 ± 0.2; *dnpc1a*^{1}, 5.0 ± 1.2; $n = 3$; $p < 0.001$) (Fig. 2*A*). The cholesterol assay is an enzyme-coupled reaction that enables the separate measurement of free cholesterol and cholesterol esters within the sample. In *dnpc1a* null mutant

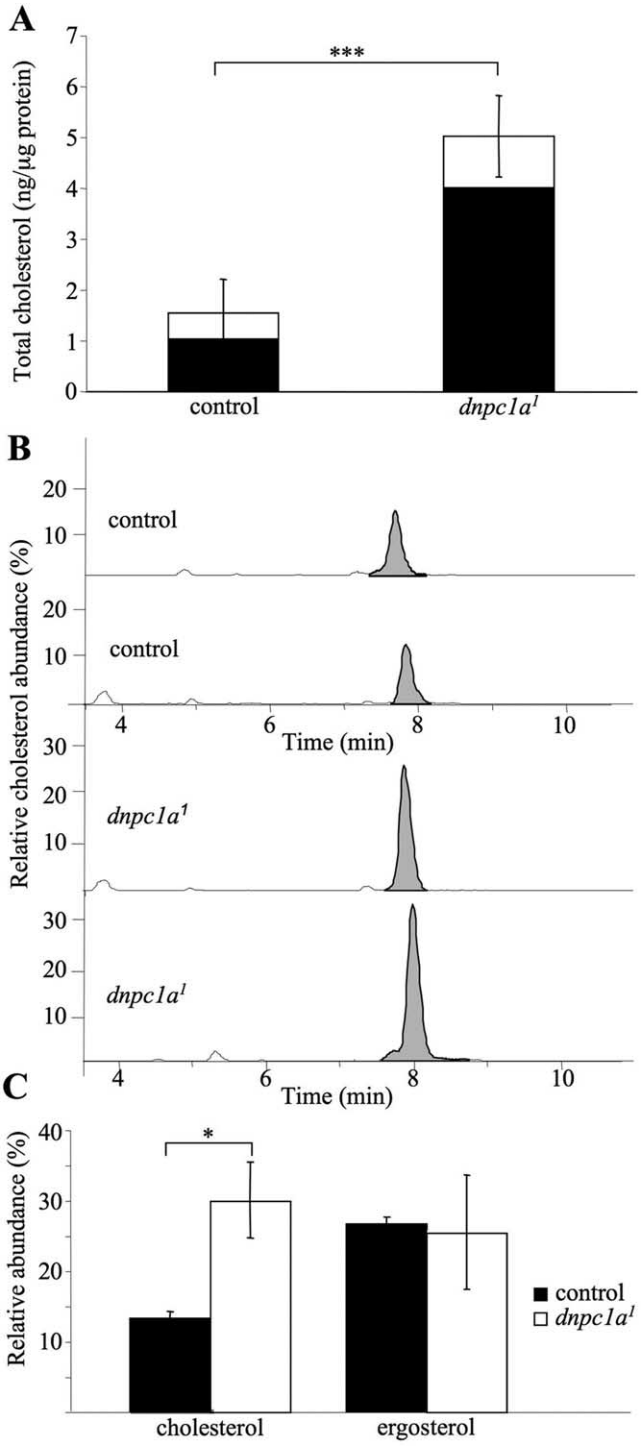

Figure 2. Cholesterol level increased in *dnpc1a* mutant brain. ***A***, Total cholesterol content of *dnpc1a* mutant heads (*dnpc1a*^{1}) is increased more than threefold compared with age-matched w^{1118} controls in the day 5 adult. Free cholesterol (black) and cholesterol esters (white) were measured separately in an enzymatic assay from head homogenates ($n = 3$). Significance is indicated at ***$p < 0.001$. ***B***, Representative HPLC–MS/MS traces of cholesterol from isolated w^{1118} control and null *dnpc1a* brains (*dnpc1a*^{1}) in the day 5 adult. Sterols from dissected brains were sulfated, resolved by HPLC, and identified in the presence of internal standard ([$^{13}C_2$]-cholesterol) by negative mode electrospray ionization MS/MS. The top two representative traces are from control brains, and the bottom two traces are from *dnpc1a* null brains. ***C***, Quantification of HPLC–MS/MS measurements of cholesterol and ergosterol. Brains from *dnpc1a* mutants (open bars) have a more than twofold increase in cholesterol levels compared with controls (filled bars), whereas ergosterol levels are not significantly different. Significance is indicated as *$p < 0.050$.

heads, there is a significant increase in both the free cholesterol ($p < 0.001$) and cholesterol esters ($p < 0.01$). However, the elevation in cholesterol esters is relatively small (Fig. 2*A*, white), with the majority of the dramatic increase in total cholesterol derived from the increase in free cholesterol content (Fig. 2*A*, black). These results indicate that dNPC1a is required to regulate cholesterol trafficking and abundance in adult heads.

To make a more quantitative assessment of the cholesterol changes specifically within the brain, mass spectrometry was used to measure sterol composition of dissected, isolated brains in *dnpc1a* mutants compared with controls (Fig. 2*B*,*C*). Mass spectrometry was done on brain lipid extracts from 7-dehydrocholesterol-fed control and mutant animals at day 5 after eclosion. Previous analyses of *Drosophila* membranes demonstrate the presence of multiple species of sterols including ergosterol, cholesterol, and dehydrocholesterol (Rietveld et al., 1999). All of these sterol species were also identified in the brain extracts in this study. Mass spectrometry was performed in the presence of an internal [$^{13}C_2$]-labeled cholesterol standard (*m/z* ratio of 467). Representative traces of cholesterol levels (*m/z* ratio of 465) from *dnpc1a* mutant and control brain lipid extracts illustrate an increase in cholesterol in null mutant brains (Fig. 2*B*). Quantification of the mass spectrometry peaks shows cholesterol greatly increased (more than twofold higher) in *dnpc1a* brains compared with age-matched controls (w^{1118} control, 13.3 ± 1.0; *dnpc1a*^{1}, 30.0 ± 5.4; $p < 0.05$) (Fig. 2*C*). This change appears specific to cholesterol, because the most abundant other sterol, ergosterol (*m/z* ratio of 475), shows no change in *dnpc1a* null brains compared with control (w^{1118} control, 26.6 ± 1.1; *dnpc1a*^{1}, 25.4 ± 8.0) (Fig. 2*C*), although there is an increased variability in ergosterol levels in the mutant brain. Thus, both enzymatic and mass spectrometry assays independently show a highly significant accumulation of cholesterol in the brain in the absence of dNPC1a function.

Filipin-positive cholesterol aggregates in *dnpc1a* null neurons

Filipin is a fluorescent polyene macrolide that binds free 3-β-hydroxysterols (Friend and Bearer, 1981), such as ergosterol and cholesterol. A hallmark phenotype of NPC mutant cells is the appearance of cholesterol aggregates revealed with filipin staining. Filipin-positive aggregates have been well documented in non-neuronal tissues in *dnpc1a* mutants, including midgut cells and the Malpighian tubules (Huang et al. 2005). With the increase in cholesterol in the *dnpc1a* null brain, we predicted a concomitant accumulation of filipin-positive aggregates in neuronal cells. We therefore assayed filipin *in situ* in brains in age-progressive studies (Fig. 3*A*) as well as in brain primary neuron cultures at the resolution of single cells (Fig. 3*B*).

The brains of "cholesterol rescued" animals were first analyzed for accumulation of filipin-positive aggregates. Isolated brains were dissected from staged, age-matched *dnpc1a* null and controls animals; lightly fixed; briefly incubated with filipin; and imaged for fluorescence. Brains from control animals at all ages (up to 45 d) exhibit only a diffuse fluorescent staining pattern, suggesting an even level of cholesterol and ergosterol distribution in all membranes (Fig. 3*A*). In sharp contrast, *dnpc1a* null brains show an obvious, age-progressive accumulation of bright filipin-positive puncta throughout the entire brain. At 5 d after eclosion, these cholesterol aggregates are already evident, but relatively scarce and mostly restricted to the cortical neuronal cell body layer at the surface of the brain (Fig. 3*A*, left). By 45 d after eclosion, intense filipin puncta are abundant throughout the entire brain of *dnpc1a* mutant animals, including all central brain

regions and the optic lobes. The filipin-positive fluorescent aggregates still amass most abundantly in association with neuronal cell bodies but are progressively also found present in the central neuropil regions (Fig. 3*A*, middle). To address the neural specificity of cholesterol aggregation, the wild-type *dnpc1a* transgene was expressed in the *dnpc1a* null mutant with the ring gland-specific −*2–286*-GAL4 driver (*dnpc1a*^{1};*2–286*-GAL4,*UAS-dnpc1a-YFP*; no neuronal expression). This expression rescues the larval lethality without cholesterol feeding but provides no rescue of the filipin-positive cholesterol aggregates in the brain (Fig. 3*A*, right). In contrast, targeted neuronal expression of the wild-type *dnpc1a* transgene in *dnpc1a* mutants with the neuron-specific *elav*-GAL4 driver (*elav*-GAL4;*dnpc1a*^{1};*UAS-dnpc1a-YFP*) strongly rescues the cholesterol aggregation defect. With neuronal expression of dNPC1a, only a small subset of brain cells shows a few detectable filipin-positive aggregates (Fig. 3*A*, right). This persistent filipin-staining pattern likely represents non-neuronal glial cells that do not express the *elav*-GAL4 driver and therefore would not express the wild-type *dnpc1a* transgene, maintaining the mutant phenotype.

Primary neuron culture provides an opportunity to image individual brain neurons at a much higher resolution (Rohrbough et al., 2003). To determine the appearance and distribution of the filipin-positive aggregates within neuronal cells, primary neuronal cultures were isolated from the brains of *dnpc1a* null mutant and control animals and imaged for filipin staining (Fig. 3*B*). Neurons derived from control animals display only faint filipin fluorescence with little or no evidence of fluorescent puncta. In sharp contrast, neurons from *dnpc1a* mutant brains clearly display an age-progressive accumulation of filipin-positive fluorescent aggregates, first within the soma but later also in neuronal processes (Fig. 3*B*). Many neuronal soma contain multiple, large fluorescent aggregates, whereas some contain one immense fluorescent aggregate. This filipin-staining pattern is quite different from that seen in mammalian NPC mutant fibroblasts and sympathetic neurons, which exhibit hundreds to thousands of tiny puncta throughout the cytoplasm (Karten et al., 2002; Reid et al., 2004). The fluorescent staining pattern in *Drosophila dnpc1a* null neurons does not resemble an endoplasmic reticulum pattern and does not colocalize with Golgi markers (e.g., GM130). Coculturing wild-type and *dnpc1a* null neurons on the same coverslip does not detectably affect the intracellular accumulation of filipin aggregates within the mutant neurons, which maintain the same large filipin-positive aggregates (Fig. 3*B*, right). The results indicate dramatic, progressive accumulation of cholesterol within aberrant neuronal organelles in the absence of dNPC1a function.

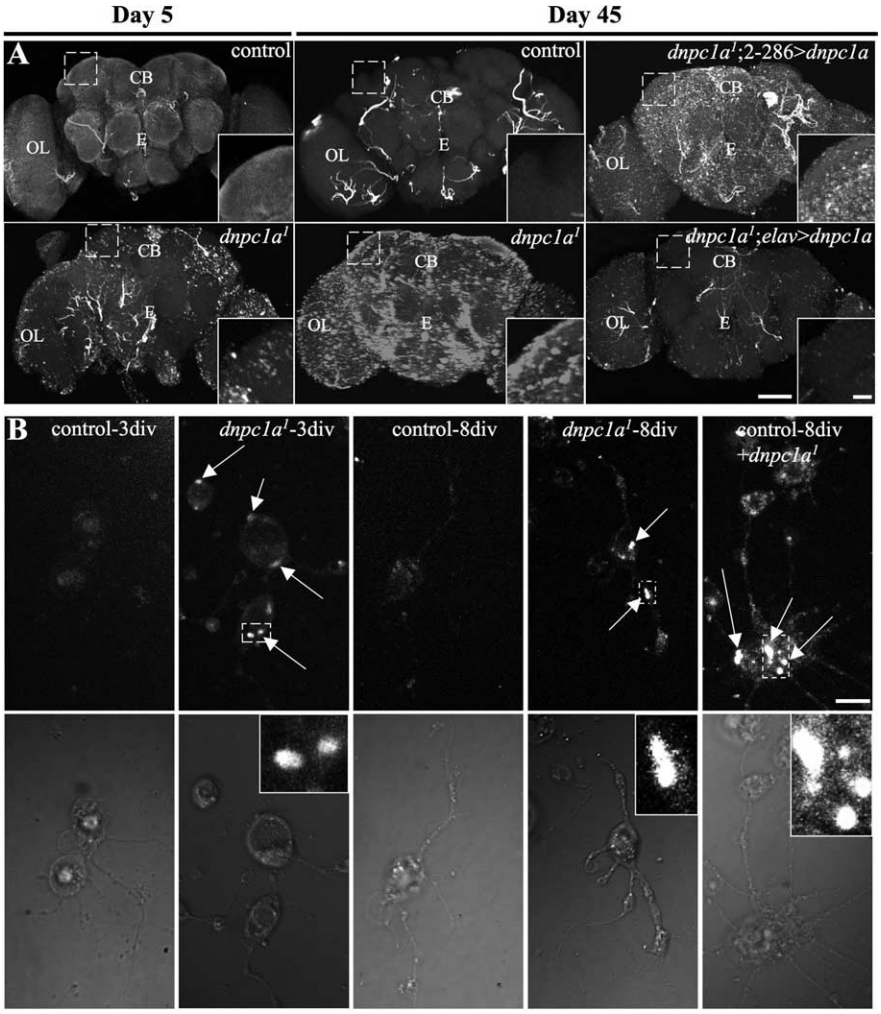

Figure 3. Age-progressive accumulation of filipin-positive cholesterol aggregates in *dnpc1a* null neurons. ***A***, Filipin-positive aggregates accumulate in the *dnpc1a* null brain in an age-progressive manner, dependent on *dnpc1a* function within brain neurons. Dissected whole brains isolated from w^{1118} control, *dnpc1a* null (*dnpc1a*^{1}), neuronally driven *elav*-GAL4;*dnpc1a*^{1};*UAS-dnpc1a-YFP* (*elav*>*dnpc1a*), and ring gland-driven *dnpc1a*^{1};*2–286*-GAL4,*UAS-npc1a-YFP* (*2–286*>*dnpc1a*) animals at the ages indicated (OL, optic lobes; CB, central brain; E, esophagus) are shown. Control brains exhibit a low-level, diffuse filipin fluorescent pattern at all ages. At day 5, *dnpc1a* null brains display fluorescent positive puncta in the optic lobes and periphery of the central brain. By day 45, the number and fluorescent intensity of filipin aggregates has greatly increased in *dnpc1a* mutants. Filipin aggregates persist in ring gland-rescued *dnpc1a* mutant brains. Filipin aggregates are greatly reduced with targeted neuronal expression of *dnpc1a* (*elav*>*dnpc1a*). Boxed regions are magnified to illustrate filipin-positive puncta. Scale bars: 100 μm; inset, 25 μm. ***B***, Live primary culture brain neurons from w^{1118} control and *dnpc1a* null (*dnpc1a*^{1}) brains. Control neurons show a low-level, hazy filipin pattern lacking puncta at all stages. Null *dnpc1a* neurons display age-progressive accumulation of fluorescent aggregates in cell bodies (white arrows) after 3 d in culture (3div). After 8 d in culture (8div), larger, more intense fluorescent aggregates are observed in both cell soma and processes (white arrows) of *dnpc1a* neurons. Coculturing control and *dnpc1a* mutant neurons on the same coverslip (control + *dnpc1a*^{1}; 8div) does not eliminate the formation of filipin-positive aggregates (white arrows) in mutant cells. Boxed regions are magnified approximately three times and placed within the differential interference contrast images. Scale bar, 5 μm.

Age-dependent neurodegeneration in *dnpc1a* null brains

The progressive loss of motor coordination, premature death, and massive accumulation of cholesterol aggregates in the brain of *dnpc1a* mutants suggests progressive neural deterioration, as in the human disease. It is therefore surprising that an early study reported no evidence of neurodegeneration in the absence of dNPC1a (Huang et al., 2005). However, this study did not indicate either the number or the age of mutant animals assayed, and because neurodegeneration is strongly predicted to be age pro-

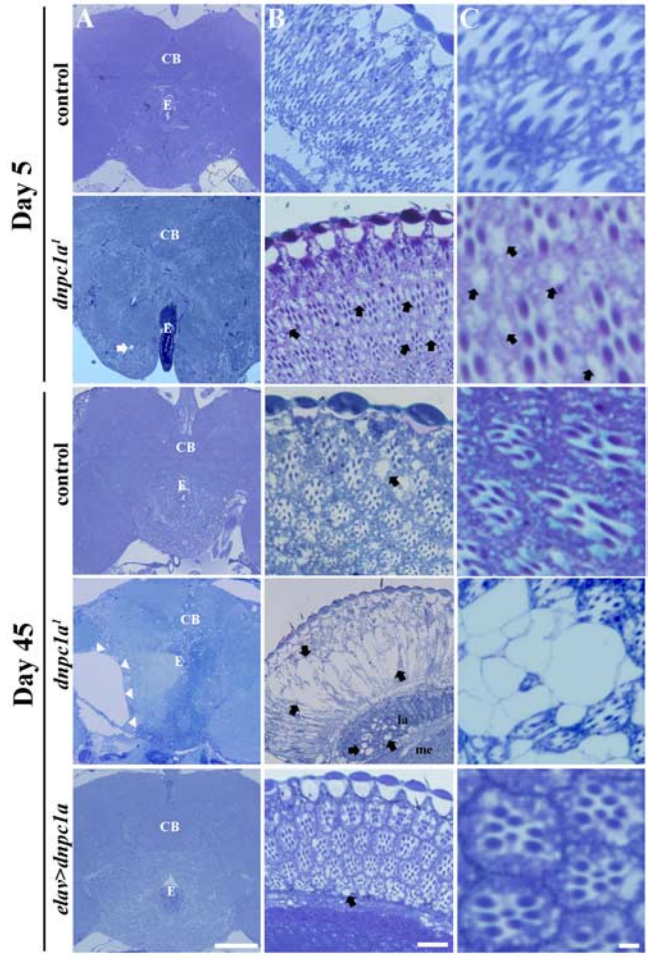

Figure 4. Age-progressive neurodegeneration in the *dnpc1a* null brain and retina. All panels show 1 μm plastic sections stained with toluidine blue. ***A***, Frontal sections of the central brain (CB) at low magnification. Control brains are mostly intact and lacking vacuoles at all ages through 45 d posteclosion. At day 5, the *dnpc1a* mutant (*dnpc1a*^{1}) brain appears essentially normal compared with w^{1118} control, with the occasional development of a small hole (arrow). By day 45, *dnpc1a* mutant brains exhibit massive tissue loss (arrowheads) and many smaller vacuoles in both neuronal soma layers and central neuropil. Targeted expression of *dncp1a* in neurons (*elav*>*dnpc1a*) totally rescues the neurodegenerative phenotype. E, Esophagus. ***B***, Frontal sections of retina at low magnification. Controls display a regular array of ommatidia, each containing seven compact rhabdomeres with surrounding cells. At day 5, the *dnpc1a* mutant (*dnpc1a*^{1}) retina is mostly intact, but small holes are beginning to form (arrows). By day 45, w^{1118} control retina also exhibit occasional small holes (arrows), but rhabdomere number and ommatidia structure remain undamaged. The day 45 *dnpc1a* null retina display massive holes (arrows) with major loss of ommatidia and rhabdomere integrity. Holes are also observed in the lamina of the optic lobe (arrows; la, lamina; me, medulla). Targeted neuronal expression (*elav*>*dnpc1a*) fully rescues the retina-degenerating phenotype in *dnpc1a* mutants. ***C***, High-magnification images of retina in ***B***. Scale bars: ***A***, 12 μm; ***B***, 6 μm; ***C***, 2 μm.

gressive, it seems likely that this previous report simply stopped short of the required level of analysis. Neurodegeneration in *Drosophila* is often characterized by vacuolization that progresses into holes large enough to be seen with light microscopy (Celotto and Palladino, 2005). We therefore began our analysis with 1 μm plastic sections through the brain in age-progressive studies in *dnpc1a* mutants and age-matched controls (Fig. 4).

Frontal sections stained with toluidine blue were made through the entire brain of *dnpc1a* null and control animals to assay the integrity of both the neuronal soma and neuropil regions. At day 5, *dnpc1a* null mutants are indistinguishable from controls, with both genotypes displaying intact neuropil and cell bodies with no detectable evidence of vacuolization (Fig. 4*A*). This result is therefore comparable to the report by Huang et al. (2005). However, analyses of day 5 *dnpc1a* retinal structures show clear signs of neurodegeneration, with the appearance of small vacuoles between clusters of undamaged ommatidia (Fig. 4*B*, magnified in 4*C*, indicated by arrows) [15 individual 1 μm sections of day 5 w^{1118} control ($n = 5$) and day 5 *dnpc1a*^{1} ($n = 4$) animals]. Ommatidia in control animals are always fully intact without any noticeable holes in retinal tissue. These results show that there is little degeneration in the young brain (5 d after eclosion) but that the retina does contain damage and therefore manifests a greater requirement for dNPC1a function.

In age-progressive studies at 5, 15, 30, and 45 d, the neurodegeneration occurring first in the retina spreads progressively and more generally throughout the brain. Frontal sections from day 15 *dnpc1a* null animals maintain primarily intact neuropil and neuronal cell soma, but now with the appearance of an occasional hole, whereas the retina exhibit clearly increased vacuolization. Examination of day 30 *dnpc1a* null sections shows a definite increase in central brain vacuolization with continuing deterioration of the retina. By day 45, frontal sections from *dnpc1a* null mutants display extensive vacuolization and massive neural tissue loss in the central brain ($n = 6$ animals; 15 1 μm sections) (Fig. 4*A*). Particularly large holes, such as shown in Figure 4*A*, were observed in multiple mutant animals and never in controls. These vacuoles are membrane bound and present in multiple sections stacked together in using NIH ImageJ software and therefore clearly do not represent a processing artifact. Age-matched control brains rarely exhibit any signs of vacuolization and never display the large cavities characteristic of null mutants ($n = 7$ animals and 15; 1 μm sections) (Fig. 4*A*).

One-micrometer-thick serial sections every 15–20 μm throughout the *dnpc1a* whole brain were generated and analyzed for the formation of vacuoles and other signs of neurodegeneration within different brain regions. Unlike other characterized *Drosophila* neurodegeneration mutants, vacuolization is not seen throughout the adult brain (Kretzschmar et al., 1997; Tschape et al., 2002). The massive tissue loss observed in day 45 *dnpc1a* mutant animals (Fig. 4*A*) always appears in very large regions in an asymmetric pattern. However, smaller holes are almost always identified in the lamina of day 45 *dnpc1a* null mutants (Fig. 4*B*). Targeted knockdown of dNPC1a in neurons achieved with a transgenic UAS-RNAi line driven by *elav*-GAL4 also demonstrates age-progressive neurodegeneration. At day 40, *dnpc1a*-RNAi animals show a more than threefold increase in vacuolization relative to age-matched controls. The quantification of vacuolated area in *dnpc1a* RNAi animals versus controls was determined by examining 5 μm hematoxylin and eosin-stained brain sections with NIH ImageJ software (control, 1.8 $\pm$ 1.1%; *dnpc1a*-RNAi, 6.8 $\pm$ 1.7%; $n > 10$ for each genotype). Consistently, *dnpc1a* null mutant animals expressing the wild-type UAS-*dnpc1a* transgene driven by *elav*-GAL4 in all neurons demonstrate a complete rescue of vacuole formation and other signs of neurodegeneration ($n = 3$ animals; 15 1 μm sections) (Fig. 4*A*). These results show that dNPC1a is required to maintain neuronal viability in the brain, specifically within neurons, as the animal ages.

In the absence of dNPC1a, vacuolization and loss of neural tissue is particularly severe in the retina. By day 45, every *dnpc1a* null mutant shows widespread vacuolization in the retina ($n = 6$ animals; 15 1 μm sections) (Fig. 4*B*,*C*). Although small holes also form in age-matched controls ($n = 7$ animals; 15 1 μm sections) (Fig. 4*B*,*C*, arrows), they are never present nearly to the extent

observed in the *dnpc1a* null retina. Thus, some photoreceptor loss does occur as a normal consequence of aging, but the onset and progression of the cell loss is dramatically increased with the loss of dNPC1a function. Furthermore, loss of rhabdomere structure is apparent throughout the retina in *dnpc1a* mutant animals (Fig. 4*B*,*C*). In many areas of *dnpc1a* null retina, there is a total loss of rhabdomere structure, whereas in other regions, rhabdomere architecture is detectable with varying degrees of membrane loss. Both the rhabdomere loss and the photoreceptor vacuolization are entirely rescued by expressing a wild-type copy of *dnpc1a* in photoreceptors with the *elav*-GAL4 driver (Fig. 4*B*,*C*). These results demonstrate that dNPC1a function is required in photoreceptors and more generally in central brain neurons to maintain viability during the later stages of animal aging.

Age-progressive ultrastructural defects in *dnpc1a* mutant neurons

A defining characteristic of NPC is the accumulation of MLBs and MVBs, extramembranous structures within the cytoplasm of NPC1 mutant cells (Liao et al., 2007). MLBs are often associated with formation of autophagic vacuoles (AVs) leading to autophagy and may represent the sites of internal cholesterol deposition occurring in the absence of NPC1 function (Bi and Liao, 2007; Pacheco et al., 2007). We used electron microscopy to examine the ultrastructural architecture of brain neuronal cells and retinal rhabdomere membrane integrity in age-progressive studies of the brain and retina in *dnpc1a* null mutants and age-matched controls (Fig. 5).

As early as day 1 after eclosion, before the onset of detectable movement defects or neurodegeneration in the central brain, neuronal cell bodies of *dnpc1a* mutants already exhibit the formation of the striking MLBs ($n = 9$ animals) (Fig. 5*A*, arrows, insets). Single MLBs, ~100–250 nm in size, are mostly found near the plasma membrane occupying ~9% of the neuronal cytoplasm. These structures are never observed in the neuronal soma of age-matched controls ($n = 5$ animals) (Fig. 5*A*). Progressive accumulation of MLBs is observed in ever increasing numbers of neuronal cell bodies over time. By day 45, the cytoplasm of nearly every *dnpc1a* mutant neuron examined contain one or more clear MLBs (occupying ~23% of the cytoplasm) or other extramembranous structures ($n = 12$ animals) (Fig. 5*A*). There is an obvious increase in the number of MLBs per neuronal cell body comparing day 5 with day 45 *dnpc1a* mutants, demonstrating age-progressive accumulation.

Similar to the difference in number of filipin-positive puncta per cell between *Drosophila* and mammalian cell cultures, there are hundreds of MLB structures in the mammalian *NPC1* mutant neuronal cell cytoplasm versus <10 in *dnpc1a* null neuronal cells (Ko et al., 2005). By day 45, immense MLBs up to 2 μm wide appear both larger and denser, with an obvious increase in the number of membrane layers, compared with day 5 and even day 30 null neurons. At day 45, expression of the wild-type UAS-*dnpc1a* transgene driven by neuron-specific *elav*-GAL4 results in a striking reduction in MLBs within the cytoplasm of all neuronal cells examined (MLBs occupy ~9% of neuronal cell cytoplasm, similar to day 5 *dnpc1a* null mutants; $n = 4$ animals) (Fig. 5*A*). However, massive MLBs, similar in size to those observed in day 45 *dnpc1a* null neurons are still clearly observed in the characteristic electron-dense glial cells (Fig. 5*A*, white arrows) that interweave their processes between neuronal cells (Fig. 5*A*, arrows in *elav*>*dnpc1a* panel). These characteristic MLB structures most likely correlate with the fluorescent aggregates seen in filipin-stained whole-brain tissues from *elav*-GAL4;*dnpc1a*^{1};*UAS-dnpc1a-YFP* animals (Fig. 3*A*). These studies show that *dnpc1a* null brain neurons display an age-progressive accumulation of exceptionally striking, multimembranous organelles that never appear in wild type and that these aberrant structures result from

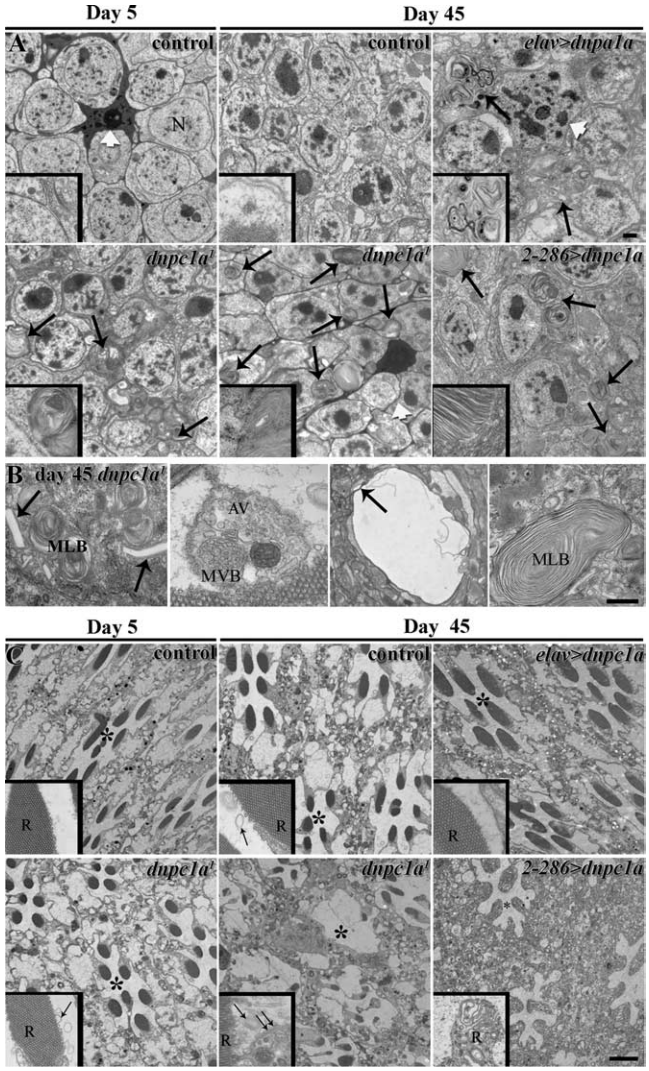

Figure 5. Targeted neuronal *dnpc1a* expression rescues ultrastructural defects. All panels show ultrathin (50–60 nm) electron microscopy sections of the brain at the ages indicated. Genotypes shown are w^{1118} control, *dnpc1a* null (*dnpc1a*^{1}), neuronally driven *elav*-GAL4; *dnpc1a*^{1};*UAS-dnpc1a-YFP* (*elav*>*dnpc1a*), and ring gland-driven *dnpc1a*^{1};*2–286*-GAL4,*UAS-npc1a-YFP* (*2–286*>*dnpc1a*). ***A***, Central brain neuronal soma. At day 5, MLBs (black arrows) are present in neuronal cell soma of *dnpc1a* mutants. By day 45, massive accumulations of MLBs (black arrows) are found in neuronal cell bodies. Control brains never produce MLBs. Targeted neuronal expression of *dnpc1a* (*elav*>*dnpc1a*) rescues MLB formation in null neurons, whereas non-neuronal cells still accumulate MLBs (white arrow, glial cell). N, Nucleus. ***B***, Ultrastructural defects commonly observed within *dnpc1a* mutant neuropil and rhabdomeres: MLB, MVB, AV, cholesterol crystal-like rods (arrows), and vacuole holes. ***C***, Ultrastructural analyses of *dnpc1a* mutant retina reveal age-progressive neurodegeneration. At day 5, both w^{1118} control and *dnpc1a* mutant (*dnpc1a*^{1}) retina exhibit distinct rhabdomeres (R) within each ommatidia; the overall architecture is intact in the *dnpc1a* mutant. Note the rhabdomere membrane invading the IRS (white arrow) in mutant. At day 45, control ommatidia remain intact with little extra membrane in the IRS, whereas *dnpc1a* mutant ommatidia exhibit large holes and loss of rhabdomere membrane integrity. High magnification shows rhabdomere degeneration and MVBs (black arrows). The architecture of day 45 ommatidia of neuronally rescued *elav*-GAL4;*dnpc1a*^{1};*UAS-dnpc1a-YFP* animals (*elav*>*dnpc1a*) is similar to age-matched controls (asterisk denotes one ommatidium), whereas ring gland-rescued *dnpc1a*^{1};*2–286*-GAL4,*UAS-dnpc1a-YFP* animals (*2–286*>*dnpc1a*) show the most severe degeneration. Scale bars: ***A***, ***B***, 500 nm; ***C***, 2 μm.

the absence of dNPC1a function within the brain neurons themselves.

Although MLBs first appear in neuronal cell bodies, in later ages, similar structures are observed within neuronal processes, consistent with concurrent appearance of filipin-positive aggregates in neuropil locations. In the neuropil of day 45 *dnpc1a* null brains, numerous MLBs are found in each electron microscope section (Fig. 5*B*). Along with the accumulation of MLBs, long crystal-like rods are commonly observed within the mutant neuropil (Fig. 5*B*, arrows in first panel). These structures closely resemble free cholesterol rods that form in model macrophage foam cells (Kellner-Weibel et al., 1999) and therefore may represent further, or more extreme, examples of cholesterol deposits. At the same age, AVs (Fig. 5*B*, second panel) and MVBs (Fig. 5*B*, fourth panel) were also commonly captured by electron microscopy imaging within the *dnpc1a* mutant central neuropil. Small membrane-bound holes are also frequently found with axon and dendritic tracts (Fig. 5*B*, arrow in third panel), reflecting loss of neuronal processes. None of these defects are ever observed in control animals and disappeared in null mutants when wild-type *dnpc1a* transgene expression is targeted to neurons with *elav*-GAL4.

Similar striking MLBs and MVBs are observed in the *dnpc1a* null retina, together with the specific loss of rhabdomere integrity (Fig. 5*C*). At day 5, both control and *dnpc1a* mutant retina maintain distinct ommatidia with typical rhabdomere structure. However, close examination of the *dnpc1a* mutant internal rhabdomere space (IRS) (Fig. 5*C*, asterisks) shows that rhabdomere membrane appears to be "swirling off" to infiltrate the IRS (Fig. 5*C*, bottom left, arrow in inset). This is a commonly observed phenotype in *dnpc1a* mutants, but only very rarely seen in controls. By day 45, *dnpc1a* mutants show extensive rhabdomere membrane intrusion into the IRS, as it deteriorates with age, and MLBs/MVBs now commonly invade the IRS (Fig. 5*C*, bottom middle panel, arrows in inset). Occasionally, rhabdomere membranes are also imaged entering the IRS in day 45 controls (Fig. 5*C*, top middle panel, arrow in inset), showing this to be a normal effect in aging, but one that is greatly enhanced in the absence of dNPC1a. Ultrastructural analyses also highlight the massive formation of holes throughout *dnpc1a* mutant ommatidia. Expression of the wild-type *dnpc1a* transgene with the ring gland-specific driver provides no detectable rescue of these striking phenotypes (Fig. 5*C*, *2–286>dnpc1a*). However, targeted neuronal expression with the *elav*-GAL4 driver (*elav>dnpc1a*) totally restores ommatidia and rhabdomere structure. These results demonstrate ultrastructural progression of membrane trafficking defects and appearance of aberrant multimembranous organelles preceding neuronal death that results from loss of dNPC1a function within neurons of the brain and retina.

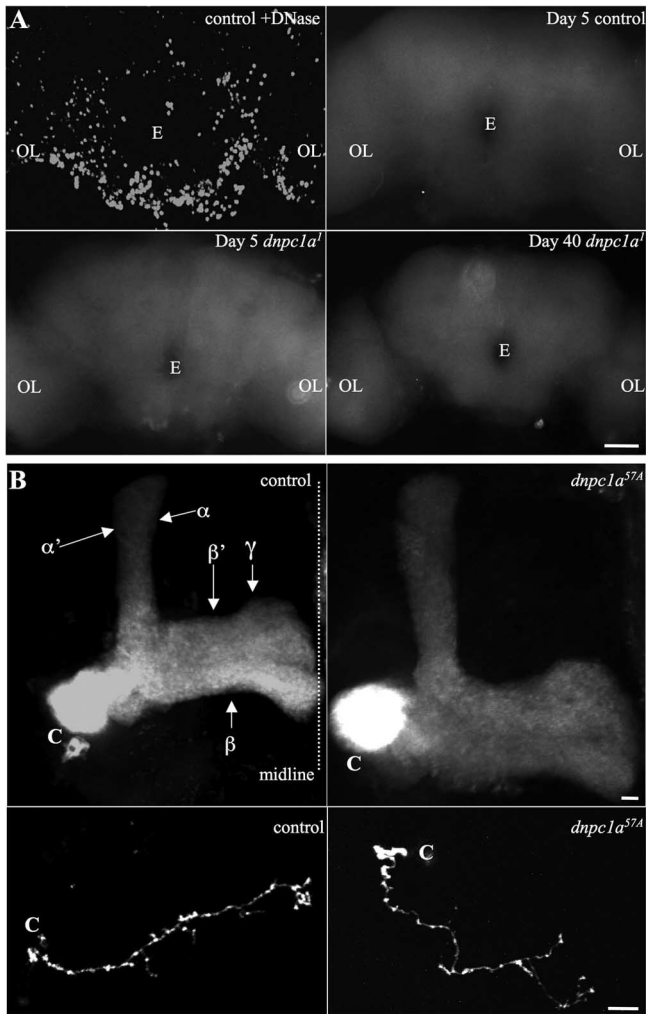

Figure 6. No evidence for apoptotic death in the *dnpc1a* null brain or a MB requirement for dNPC1a. ***A***, No evidence of apoptotic death in brains of *dnpc1a* mutants. w^{1118} control brains treated with DNase exhibit robust TUNEL staining, whereas untreated controls are negative for TUNEL-positive nuclei. Day 5 and 45 *dnpc1a* mutants ($dnpc1a^{1}$) show no detectable TUNEL-positive apoptotic nuclei. OL, Optic lobes; E, esophagus. ***B***, Top, The brain MB labeled with MARCM UAS-CD8-GFP driven by GAL4-OK107. The α/α', β/β', and γ axonal lobes and location of Kenyon cell bodies (C) and brain midline (dotted line) are indicated. MB morphology of large MARCM *dnpc1a* null clones ($dnpc1a^{1}$) at day 45 is indistinguishable from w^{1118} control clones. Bottom, Single MARCM clones of γ neurons are shown for control and *dnpc1a* null at day 50. The single MARCM *dnpc1a* mutant γ neuron extends normally into the MB γ lobe and maintains architecture comparable to the control neuron. Scale bars: ***A***, 50 μm; ***B***, top, 5 μm; bottom, 10 μm.

Age-progressive neurodegeneration without apoptosis in *dnpc1a* mutant brains

It is not clear whether the neurodegeneration characterizing NPC results from programmed apoptosis or some form of necrotic cell death. Low numbers of apoptotic cells are detected in the cerebrum and cerebellum of human patients and the mouse model of NPC (Wu et al., 2005). A recent study of *npc2* mutants in *Drosophila* similarly reveals apoptotic cell death in the brain (Huang et al., 2007). Conflicting data have demonstrated that Purkinje cell (PC) neuron loss in $npc1^{-/-}$ mutant mice cannot be delayed with apoptotic inhibitors, either genetically or pharmacologically (Erickson and Bernard, 2002). We therefore assayed *dnpc1a* mutant brains for the presence of apoptotic cells by TUNEL staining in age-progressive studies (Fig. 6*A*).

Very few apoptotic cells are observed in control adult brains at any age. Therefore, as a positive control, wild-type brains were treated with DNase to reveal intense TUNEL-positive apoptotic nuclei residing in the cortical neuronal soma layer around the periphery of the brain (Fig. 6*A*). Null *dnpc1a* mutant brains were examined for TUNEL labeling in both young adult (day 5) and late-age adult (day 45). Neither stage showed any detectable TUNEL labeling indicative of apoptosis (Fig. 6*A*). In fact, TUNEL staining appears remarkably similar in mutants and age-matched controls. These results show that the neurodegeneration caused by loss of dNPC1a in the brain is not characterized by the TUNEL labeling indicating apoptosis.

The dNPC1a requirement is not cell autonomous or brain region specific

A chimeric mouse model shows that PC neurons lacking NPC1 continue to die when surrounded by normal cells (Ko et al., 2005), suggesting that the mutant neuronal cell loss is a cell-autonomous process. The above results presented here also clearly show that the dNPC1a requirement is within neuronal cells and that glia interspersed among neurons expressing a wild-type *dnpc1a* transgene continue to manifest the full range of cholesterol accumulation and ultrastructural mutant defects. Conversely, expression of wild-type *dnpc1a* in non-neuronal ring gland tissue provides no rescue. These data collectively suggest a cell-autonomous requirement for dNPC1a function. To test this hypothesis, and to determine the effect of loss of dNPC1a on neuron morphology at the single-cell level, we used the mosaic analysis with repressible cell marker (MARCM) technique (Lee and Luo, 1999) to generate homozygous *dnpc1a* mutant clones in an otherwise wild-type brain (Fig. 6*B*).

The MB-specific OK107-GAL4 driver was first used to target *dnpc1a* null mutant clones to this well defined brain region (Connolly et al., 1996). The MB possesses a clear dendritic region (calyx) and five distinct axon lobes (Fig. 6*B*). There are three classes of MB Kenyon cell neurons: γ (projection of a single horizontal axon) and α/β and α'/β' (two axon projections, one horizontal and one vertical) (Lee et al., 1999) (Fig. 6*B*). By targeting the developmental period of mutant clone induction, MB clones can be made from the size of hundreds of neurons down to a single mutant neuron clone. Surprisingly, large MB *dnpc1a* null mutant clones show no consistent difference from wild-type clones in the maintenance of overall MB morphology or the architecture of the extensive axonal projections (Fig. 6*B*, top). In age-progressive studies through day 50, the large MB MARCM mutant clones show no detectable signs of apoptosis or cell loss that might indicate cell death or neurodegeneration. Therefore, single-cell MB MARCM clones were generated to observe individual cell bodies, dendrites, and axonal projections. Detailed analysis of single-cell MARCM *dnpc1a* γ neurons show no overt differences compared with wild-type single-cell MARCM clones (Fig. 6*B*, bottom). Further analysis of α/β and α'/β' *dnpc1a* single-cell MARCM clones show no age-dependent effect such as process loss or cell death. These results suggest either that the requirement for dNPC1a within the brain is not cell autonomous or that the *dnpc1a* requirement is neuron-type specific and that MB neurons manifest a low requirement for dNPC1a.

To further examine the requirement of dNPC1a in other regions of the brain and retina, the MARCM technique was used to generate randomly induced *dnpc1a*^{1} mutant clones more generally. To this end, the pan-neuronal *elav*-GAL4 driver was used instead of the MB-specific OK107-GAL4 driver. We were unable to generate very large *dnpc1a* null clones. However, induced *dnpc1a* null clones randomly located throughout the central brain of day 30 animals clearly colocalize with accumulations of cholesterol aggregates as monitored by filipin staining (Fig. 7*A*, bottom, white arrows). Age-matched control brains demonstrate no accumulation of filipin-positive puncta (Fig. 7*A*, top). We further analyzed *elav*-GAL4 MARCM *dnpc1a* null clones by electron microscopy for the formation of MLVs or vacuoles that are easily identifiable in *dnpc1a* mutant animals. Control MARCM brains exhibited no accumulation of MLBs or MVBs in neuronal cell bodies (Fig. 7*B*). In contrast, the *elav*-GAL4-driven MARCM *dnpc1a* mutant neuronal cell bodies accumulate MLBs (Fig. 7*B*, black arrows), whereas adjacent wild-type neurons maintain normal cytoarchitecture. Thus, both the sterol accumulation and membrane trafficking defects characteristic of dying neurons clearly manifest a cell-autonomous requirement widely throughout the nervous system.

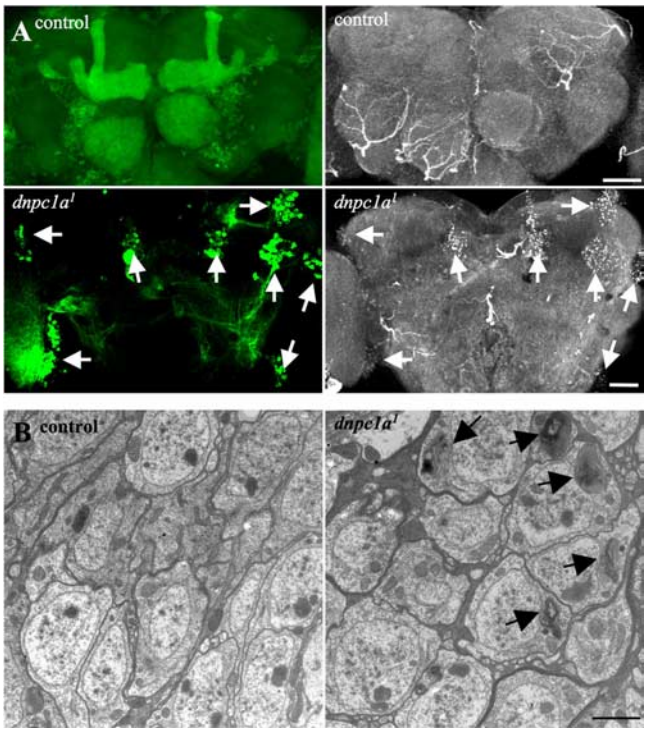

Figure 7. Null *dnpc1a* mutant neuron clones display cell-autonomous requirements in cholesterol trafficking and neuronal maintenance. ***A***, Central brain labeled with MARCM UAS-CD8-GFP driven by *elav*-GAL4 and filipin staining for sterol aggregates. Top panels show wild-type control MARCM whole-brain clones, whereas bottom panels show randomly generated *dnpc1a* null mutant clones. Null *dnpc1a* clones are green fluorescent protein (GFP) positive (bottom left, white arrows) and colocalize with cholesterol-rich, filipin-positive aggregates (bottom right, white arrows). Whole-brain MARCM control neurons are all GFP positive (top left) and display a diffuse low level of filipin staining with no puncta (top right). All brains are aged to 30 d posteclosion. ***B***, Panels show ultrathin (50–60 nm) electron microscopy sections of *elav*-GAL4 MARCM brains in control (left) and *dnpc1* null (right). MARCM *dnpc1a* mutant clones accumulate numerous MLBs (black arrows) in neuronal cell soma, whereas adjacent cells show normal ultrastructure. MARCM controls display no MLBs in neuronal soma. All brains are aged to 30 d posteclosion. Scale bars: ***A***, 50 μm.; ***B***, 2 μm.

Age-dependent loss of neuronal function in the *dnpc1a* null visual system

Drosophila neurodegeneration models have usually not used electrophysiological methods to assay neuronal function, and yet this is perhaps the most sensitive and quantitative measure of neuronal integrity. One classic method is ERG recording of the light-evoked currents of photoreceptors, occurring as a sustained negative response during phototransduction (Heisenberg, 1971). The ERG also records on- and off-transients at the beginning and end of the light stimulus, representing the postsynaptic L1 and L2 monopolar lamina cell responses to photoreceptor synaptic transmission (Coombe, 1986). Thus, this single measurement allows the assay of both photoreceptor functional viability and the persistence of synaptic connectivity in the visual system. We recorded ERGs in age-progressive studies comparing *dnpc1a* null mutants to age-matched controls (Fig. 8).

In young animals (day 5), both mutant and control show rapid and sustained photoreceptor depolarization during a light stimulus. Representative ERG recordings are shown in

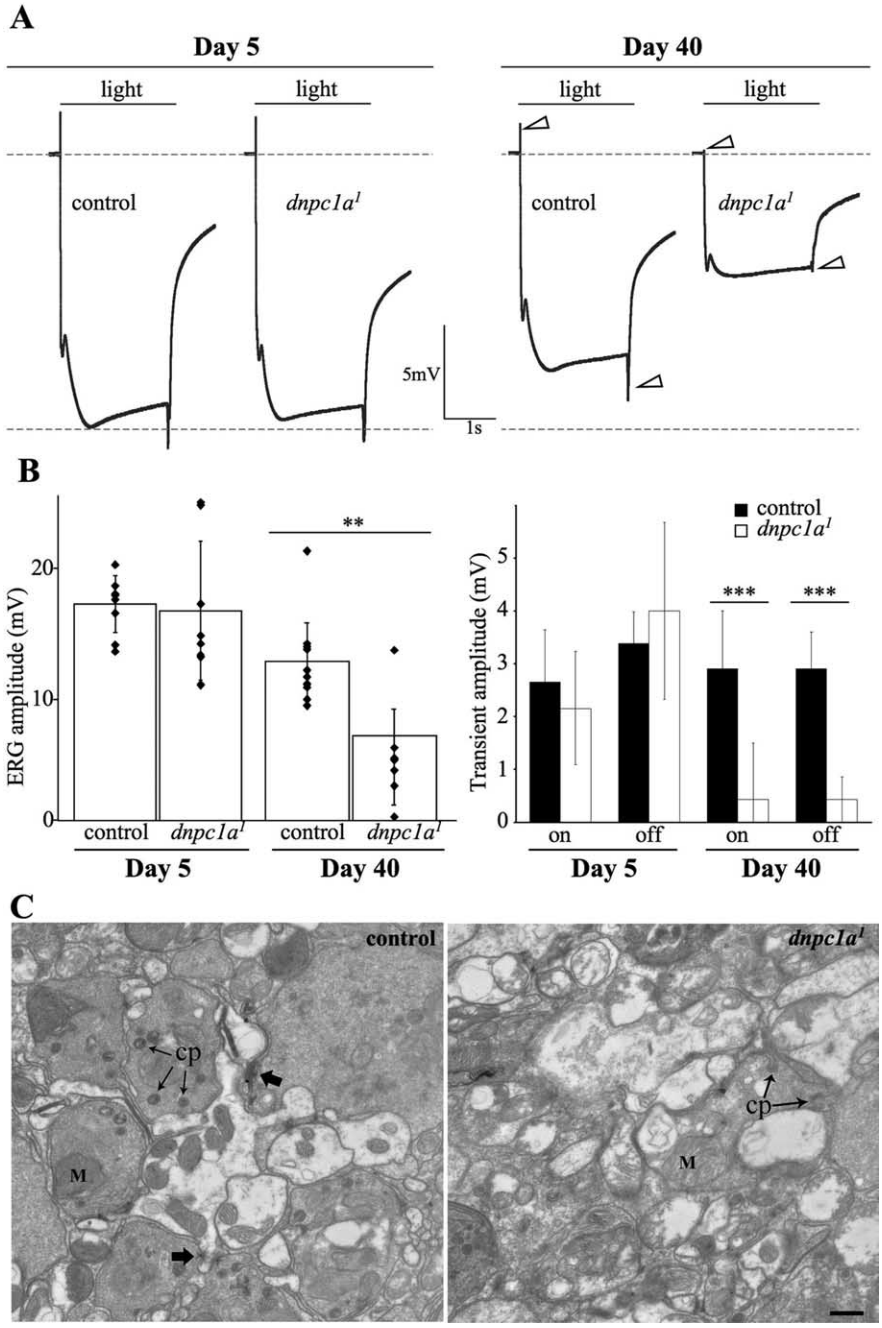

Figure 8. Age-progressive loss of neuron and synapse function in *dnpc1a* retina. ***A***, Representative ERG recordings in response to a 2 s light flash, showing sustained phototransduction responses and the lights on/off synaptic transients in *dnpc1a* mutants (*dnpc1a*^{1}) and w^{1118} controls at the ages indicated. At day 5, control and *dnpc1a*^{1} mutants show equal sustained negative responses and synaptic transients. By day 40, ERG amplitudes of control animals are attenuated compared with day 5 controls, but the *dnpc1a* mutants show a very dramatic further reduction compared with age-matched controls. The synaptic transients of day 45 *dnpc1a* mutants are almost totally lost (arrowheads). ***B***, Quantification of ERG and synaptic transient amplitudes is shown for day 5 and day 40 animals. Each graph shows a scatter plot of individual ERG amplitudes (diamonds; n = at least 6 animals per condition) with a histogram bar showing mean ± SD. Significance is indicated as $^{**}p < 0.01$ and $^{***}p < 0.001$. ***C***, Electron microscopy cross sections of control and *dnpc1a* mutant photoreceptor lamina cartridges. The organization of the *dnpc1a* mutant cartridge is deranged with holes, MLBs, and very few synaptic capitate projections (cp). Synaptic active zones (arrows) and mitochondria (M) are marked. Scale bar, 500 nm.

response to a 2 s light flash for the control and *dnpc1a* null (Fig. 8*A*, left), revealing indistinguishable depolarization responses. Quantification of the sustained ERG amplitudes (Fig. 8*B*, left) (w^{1118} control: 17.3 ± 2.3, $n = 8$; *dnpc1a*^{1}: 16.8 ± 5.6, $n = 8$) shows that *dnpc1a* mutants exhibit normal phototransduction early in life. In aged animals at 40 d, the situation has changed dramatically. In control animals, aging results in a slight reduction in mean ERG amplitude at day 40 compared with day 5 (Fig. 8*A*, right). However, *dnpc1a* mutant animals show a much greater age-dependent loss of phototransduction, with a 50% decrease in ERG amplitude compared with the age-matched controls (Fig. 8*A*). Quantification of day 40 ERG amplitudes reveal a significant reduction in *dnpc1a* null mutants compared with age-matched controls (w^{1118} control: 12.4 ± 3.0, $n = 10$; *dnpc1a*^{1}: 6.7 ± 3.7, $n = 7$; $p < 0.01$) (Fig. 8*B*). Mutant animals exhibit a wide range of ERG amplitudes, with one response in the wild-type range and all others with little to no response to light stimulus. This is in agreement with the variation observed in toluidine blue and electron microscopy images of mutant retina, showing severe retina and rhabdomere degeneration but also regions of relatively preserved ommatidia and rhabdomere integrity.

In young animals, day 5 control and *dnpc1a* mutants display comparable synaptic on- and off-transients. In contrast, age also causes a dramatic loss of synaptic on- and off-transients in *dnpc1a* mutant ERG recordings compared with age-matched controls (Fig. 8*A*, right, arrowheads). At day 40, the on- and off-transients are almost nonexistent in representative *dnpc1a* mutant traces. Quantification of on/off synaptic transients from day 40 animals demonstrates a highly significant ($p < 0.001$) reduction in synaptic transients in *dnpc1a* mutants compared with controls (w^{1118} control: on-transient, 2.9 ± 1.1; off-transient, 2.9 ± 1.0; *dnpc1a*^{1}: on-transient, 0.4 ± 0.7; off-transient, 0.4 ± 0.4) (Fig. 8*B*, right). This particularly severe functional defect in synaptic transmission suggests specific defects within the photoreceptor synaptic cartridge. Ultrastructural examination of photoreceptor cartridges reveals the accumulation of MLBs in intact cells and a high incidence of vacuoles in *dnpc1a* mutants (Fig. 8*C*). Where the photoreceptor terminates into the cartridge, capitate projections (CPs), sites of synaptic vesicle endocytosis, extend from the invagination of glia into the synaptic terminal (Fabian-Fine et al., 2003). Null *dnpc1a* terminals display very few CP structures (Fig. 8*C*), consistent with the severe loss of synaptic transmission. Thus, assays coupling measures of neuronal function with anatomical observations combine to show age-progressive neurodegeneration in the absence of dNPC1a.

Discussion

Drosophila models of human neurodegenerative diseases have made substantial inroads toward elucidating underlying cellular, molecular, and genetic dysfunction (Palladino et al., 2003; Tschape et al., 2003; Celotto and Palladino, 2005; Dermaut et al., 2005; Hickey et al., 2006). These models can be further strengthened by the addition of the imaging resolution of brain primary neuronal cultures, detailed electron microscopy analyses of neuronal ultrastructural and electrophysiology assays of neuronal function during disease progression. The breadth of these new tactics greatly enhances our repertoire of approaches to provide insights into neurodegenerative disease states. In this study, we bring together this broad-spectrum strategy to generate a comprehensive model of NPC.

Ninety-five percent of NPC disease cases are caused by mutation of NPC1, a 13-pass transmembrane protein that resides in a unique class of endosomal organelles, binds cholesterol, and has the hallmarks of a transporter involved in sphingolipid/cholesterol trafficking (Mukherjee and Maxfield, 2004; Scott and Ioannou, 2004; Vance et al., 2006). Loss of the *Drosophila* ortholog dNPC1a has been reported previously to result in early lethality attributable to the loss of cholesterol-dependent ecdysone production, a steroid hormone required for molting (Huang et al., 2005; Fluegel et al., 2006). This insect-specific requirement has been a distraction, and has prevented detailed characterization of the *Drosophila* model. Fortunately, this early block in development is easily bypassed through a diet of excess ecdysone precursors (cholesterol or 7-dehydrocholesterol) or by targeted expression of dNPC1a in the ring gland, the endocrine organ that produces ecdysone (Thummel, 1996). Null *dnpc1a* mutants rescued to adulthood show progressive locomotor defects, greatly reduced life span, intracellular accumulation of cholesterol aggregates, and age-progressive neurodegeneration, a constellation of phenotypes that closely mimic the human NPC disease condition (Sturley et al., 2004; Walkley and Suzuki, 2004). Importantly, all of these phenotypes are rescued by targeted neuronal expression of dNPC1a in the null mutant, demonstrating a neural requirement.

Previous reports conclude that loss of dNPC1a does not cause neurodegeneration (Huang et al., 2005; Fluegel et al., 2006). In contrast, we show here that the lack of dNPC1a within the brain causes the age-progressive accumulation of massive intracellular membranous structures, which are never observed in wild-type neurons, and brain degeneration starting as small vacuoles within the retina and progressing to massive tissue loss within both the retina and central brain. Similar neurodegeneration occurs in *dnpc1a* null mutants fed high levels of cholesterol during larval growth or expressing wild-type *dnpc1a* in the ring gland. Thus, neither cholesterol feeding nor ecdysone function contributes to the *dnpc1a* neurodegeneration phenotypes. In *Drosophila*, dNPC1a-dependent steroid hormone expression clearly explains the requirement for dNPC1a during development (Huang et al., 2005). Similarly in mammals, loss of NPC1 is associated with lower neurosteroid levels, and administration of the neurosteroid allopregnanolone reportedly delays onset of neurological symptoms in NPC1$^{-/-}$ mice (Griffin et al., 2004; Langmade et al., 2006). These data clearly argue for NPC1-dependent generation of cholesterol-derived signaling steroids. However, characterized steroid hormones in *Drosophila* derive from the ring gland, and we show that dNPC1a function in the ring gland provides no protection against neurodegeneration.

Targeted neuronal expression of wild-type NPC1 in both the murine and *Drosophila* models prevents neurodegeneration associated with NPC1 dysfunction (Loftus et al., 2002). The *elav*-GAL4-driven expression of wild-type dNPC1a does not lead to glial cell transgene expression. The neurodegenerative process in NPC cases has been linked to glial cell and astrocyte cellular dysfunction because of NPC1 localization to these cell types (Patel et al., 1999; German et al., 2002). However, in the neuronal dNPC1a rescue animals, glial cells lacking dNPC1a adjacent to neurons expressing wild-type dNPC1a still accumulate massive MLBs and filipin-positive puncta. It is presently not known whether these glial cells die. Nevertheless, targeted glial expression of dNPC1a clearly provides significant rescue for the early-onset lethality of *dnpc1a* mutants, demonstrating that dNPC1a function in glia plays a substantial role in this disease model. Thus, in *Drosophila* dNPC1a function in both glia and neurons is important for prolonged survival during aging.

Chimeric mice with functional dNPC1 expressed in a few cells still manifest death of nearby *npc1* mutant neurons (Ko et al., 2005), at least suggesting a cell-autonomous role for NPC1 in neuronal cell survival. However, in *Drosophila*, our MARCM clonal results show that MB neurons apparently do not require dNPC1a for long-term survival. MARCM analyses of aged day 50 *dnpc1a* null neurons show intact neuronal perikarya, elaborate dendrites, and structurally mature axons. These data, along with the neurodegenerative delay associated with neurosteroid application to *npc1*$^{-/-}$ mutants early in murine development, argue for a non-cell-autonomous role for NPC1 function. In contrast, MARCM analysis of randomly induced *dnpc1a* null clones throughout the brain clearly demonstrates a cell-autonomous accumulation of cholesterol aggregates, as revealed by filipin staining, and the formation of extensive MLBs in neuronal soma, characteristic of ailing cells. It remains formally possible that steroids produced by neurons depend on dNPC1a function and that such neurosteroids maintain neuronal viability and so guard against complete neurodegeneration. Furthermore, although almost all neurons in the NPC$^{-/-}$ mice are filipin positive, not all neurons are equally vulnerable, because there are low levels of neuron loss in the thalamous and prefrontal cortex in the face of nearly complete PC loss (German et al., 2001). Similarly, in the *Drosophila* brain, it appears that some neuron populations are also more sensitive to the loss of dNPC1a, at least at the level of full cellular death.

Loss of dNPC1a function in *Drosophila* neurons strongly impacts cholesterol trafficking. Null *dnpc1a* brains accumulate highly elevated levels of cholesterol and cholesterol aggregates at exceedingly high levels within aberrant neuronal organelles. These MLB structures are often composed of hundreds of layers of wrapped membrane and accumulate progressively in both size and abundance in all neurons in the absence of dNPC1a. Whereas the existence and formation of MLBs is not always a pathological symptom, the massive accumulation of MLBs seen in a variety of disease conditions is clearly an indication of severe cellular dysfunction (Schmitz and Muller, 1991). It has been proposed that sphingolipid storage disease cells upregulate a Beclin-1-regulated autophagic process (self-digestion) to promote cell survival (Pacheco et al., 2007). The formation of cholesterol-rich MLBs seen in NPC1-deficient cells is consistent with such autophagic cell death.

The cytoplasmic accumulation of MLBs in neurons is observed in a variety of other *Drosophila* mutants, also associated with adult lethality, neurodegeneration, and synaptic dysfunction. The formation of MLBs in the retina and neuromuscular synaptic junction are neuronal phenotypes in the *bench-*

warmer (*bnch*) mutant, caused by loss of a predicted lysosomal sugar carrier (Dermaut et al., 2005). The *eggroll* mutant exhibits similar MLB structures in neurons and glial cells, with associated brain vacuolization and early-onset lethality (Min and Benzer, 1997). A *Drosophila* disease model for infantile neuronal ceroid lipofuscinoses (*Ppt1* mutants) displays the same accumulation of MLBs throughout the brain, with associated early lethality but without reported signs of brain vacuolization or neuronal tissue loss (Hickey et al., 2006). The genetic lesion causing *eggroll* has yet to be determined, but *dnpc1a*, *bnch*, and *Ppt1* are all lysosomal/endosomal proteins, clearly linking neuronal MLB formation with endosomal trafficking defects.

Sterols (ergosterol and cholesterol) together with sphingolipids are the major components of lipid rafts. *Drosophila* lipid rafts are important for the light-induced recruitment of INAD-signaling phototransduction complexes in photoreceptors (Sanxaridis et al., 2007) and also act as positive regulators of the *Drosophila* metabotropic glutamate receptor (DmGluRA) signaling between neurons (Eroglu et al., 2003). *Drosophila* lipid rafts also regulate voltage-gated ion channel signaling and the synaptic vesicle cycling underlying neurotransmission (Rohrbough et al., 2004; Gasque et al., 2005; Rohrbough and Broadie, 2005). Altering cholesterol levels and trafficking within neurons presumably has a great impact on membrane lipid rafts and their dependent mechanisms. Loss of NPC1 is linked to the depletion of lipid rafts in endocytic membranes (Simons and Gruenberg, 2000; Lusa et al., 2001). Loss of dNPC1a causes profound changes in cholesterol distribution and thus likely also disrupts lipid rafts. We show here that loss of dNPC1a disrupts relevant neuronal processes, including phototransduction in retinal photoreceptors and synaptic transmission to the optic lamina. The *Drosophila* NPC1 model is a good system to investigate whether NPC1 regulates formation or maintenance of lipid rafts in neurons, which may in turn be required for neuronal function and viability. Genetic and proteomic screens can tease out other players in the lipid trafficking pathway and thus provide insight into the dysfunction driving intracellular cholesterol/sphingolipid accumulation (Byun et al., 2006; Reddy et al., 2006) and identify potential drug targets for alleviating the catastrophic consequences of the NPC disease.

References

Beltroy EP, Richardson JA, Horton JD, Turley SD, Dietschy JM (2005) Cholesterol accumulation and liver cell death in mice with Niemann-Pick type C disease. Hepatology 42:886–893.

Bi X, Liao G (2007) Autophagic-lysosomal dysfunction and neurodegeneration in Niemann-Pick type C mice: lipid starvation or indigestion? Autophagy 3:646–648.

Bligh EG, Dyer WJ (1959) A rapid method of total lipid extraction and purification. Can J Biochem Physiol 37:911–917.

Byun K, Kim J, Cho SY, Hutchinson B, Yang SR, Kang KS, Cho M, Hwang K, Michikawa M, Jeon YW, Paik YK, Lee B (2006) Alteration of the glutamate and GABA transporters in the hippocampus of the Niemann-Pick disease, type C mouse using proteomic analysis. Proteomics 6:1230–1236.

Carstea ED, Morris JA, Coleman KG, Loftus SK, Zhang D, Cummings C, Gu J, Rosenfeld MA, Pavan WJ, Krizman DB, Nagle J, Polymeropoulos MH, Sturley SL, Ioannou YA, Higgins ME, Comly M, Cooney A, Brown A, Kaneski CR, Blanchette-Mackie EJ, et al. (1997) Niemann-Pick C1 disease gene: homology to mediators of cholesterol homeostasis. Science 277:228–231.

Celotto AM, Palladino MJ (2005) *Drosophila*: a "model" model system to study neurodegeneration. Mol Interv 5:292–303.

Connolly JB, Roberts IJ, Armstrong JD, Kaiser K, Forte M, Tully T, O'Kane CJ (1996) Associative learning disrupted by impaired Gs signaling in *Drosophila* mushroom bodies. Science 274:2104–2107.

Coombe PE (1986) The large monopolar cells L1 and L2 are responsible for ERG transients in *Drosophila*. J Comp Physiol A Neuroethol Sens Neural Behav Physiol 159:655–665.

Davies JP, Ioannou YA (2000) Topological analysis of Niemann-Pick C1 protein reveals that the membrane orientation of the putative sterol-sensing domain is identical to those of 3-hydroxy-3-methylglutaryl-CoA reductase and sterol regulatory element binding protein cleavage-activating protein. J Biol Chem 275:24367–24374.

Dermaut B, Norga KK, Kania A, Verstreken P, Pan H, Zhou Y, Callaerts P, Bellen HJ (2005) Aberrant lysosomal carbohydrate storage accompanies endocytic defects and neurodegeneration in *Drosophila* benchwarmer. J Cell Biol 170:127–139.

Erickson RP, Bernard O (2002) Studies on neuronal death in the mouse model of Niemann-Pick C disease. J Neurosci Res 68:738–744.

Eroglu C, Brugger B, Wieland F, Sinning I (2003) Glutamate-binding affinity of *Drosophila* metabotropic glutamate receptor is modulated by association with lipid rafts. Proc Natl Acad Sci USA 100:10219–10224.

Fabian-Fine R, Verstreken P, Hiesinger PR, Horne JA, Kostyleva R, Zhou Y, Bellen HJ, Meinertzhagen IA (2003) Endophilin promotes a late step in endocytosis at glial invaginations in *Drosophila* photoreceptor terminals. J Neurosci 23:10732–10744.

Finley KD, Edeen PT, Cumming RC, Mardahl-Dumesnil MD, Taylor BJ, Rodriguez MH, Hwang CE, Benedetti M, McKeown M (2003) blue cheese mutations define a novel, conserved gene involved in progressive neural degeneration. J Neurosci 23:1254–1264.

Fluegel ML, Parker TJ, Pallanck LJ (2006) Mutations of a *Drosophila* NPC1 gene confer sterol and ecdysone metabolic defects. Genetics 172:185–196.

Freeman MR, Doherty J (2006) Glial cell biology in *Drosophila* and vertebrates. Trends Neurosci 29:82–90.

Friedland N, Liou HL, Lobel P, Stock AM (2003) Structure of a cholesterol-binding protein deficient in Niemann-Pick type C2 disease. Proc Natl Acad Sci USA 100:2512–2517.

Friend DS, Bearer EL (1981) beta-Hydroxysterol distribution as determined by freeze-fracture cytochemistry. Histochem J 13:535–546.

Garver WS, Heidenreich RA, Erickson RP, Thomas MA, Wilson JM (2000) Localization of the murine Niemann-Pick C1 protein to two distinct intracellular compartments. J Lipid Res 41:673–687.

Gasque G, Labarca P, Darszon A (2005) Cholesterol-depleting compounds modulate K+-currents in *Drosophila* Kenyon cells. FEBS Lett 579:5129–5134.

German DC, Quintero EM, Liang CL, Ng B, Punia S, Xie C, Dietschy JM (2001) Selective neurodegeneration, without neurofibrillary tangles, in a mouse model of Niemann-Pick C disease. J Comp Neurol 433:415–425.

German DC, Liang CL, Song T, Yazdani U, Xie C, Dietschy JM (2002) Neurodegeneration in the Niemann-Pick C mouse: glial involvement. Neuroscience 109:437–450.

Griffin LD, Gong W, Verot L, Mellon SH (2004) Niemann-Pick type C disease involves disrupted neurosteroidogenesis and responds to allopregnanolone. Nat Med 10:704–711.

Heisenberg M (1971) Separation of receptor and lamina potentials in the electroretinogram of normal and mutant *Drosophila*. J Exp Biol 55:85–100.

Hickey AJ, Chotkowski HL, Singh N, Ault JG, Korey CA, MacDonald ME, Glaser RL (2006) Palmitoyl-protein thioesterase 1 deficiency in *Drosophila melanogaster* causes accumulation of abnormal storage material and reduced life span. Genetics 172:2379–2390.

Huang FD, Matthies HJ, Speese SD, Smith MA, Broadie K (2004) Rolling blackout, a newly identified PIP2-DAG pathway lipase required for *Drosophila* phototransduction. Nat Neurosci 7:1070–1078.

Huang X, Suyama K, Buchanan J, Zhu AJ, Scott MP (2005) A *Drosophila* model of the Niemann-Pick type C lysosome storage disease: dnpc1a is required for molting and sterol homeostasis. Development 132:5115–5124.

Huang X, Warren JT, Buchanan J, Gilbert LI, Scott MP (2007) *Drosophila* Niemann-Pick Type C-2 genes control sterol homeostasis and steroid biosynthesis: a model of human neurodegenerative disease. Development 134:3733–3742.

Infante RE, Radhakrishnan A, Abi-Mosleh L, Kinch LN, Wang ML, Grishin NV, Goldstein JL, Brown MS (2007) Purified NPC1 protein: II. Localization of sterol binding to a 240-amino acid soluble luminal loop. J Biol Chem 283:1064–1075.

Jiang SA, Campusano JM, Su H, O'Dowd DK (2005) *Drosophila* mushroom

body Kenyon cells generate spontaneous calcium transients mediated by PLTX-sensitive calcium channels. J Neurophysiol 94:491–500.
Karten B, Vance DE, Campenot RB, Vance JE (2002) Cholesterol accumulates in cell bodies, but is decreased in distal axons, of Niemann-Pick C1-deficient neurons. J Neurochem 83:1154–1163.
Kellner-Weibel G, Yancey PG, Jerome WG, Walser T, Mason RP, Phillips MC, Rothblat GH (1999) Crystallization of free cholesterol in model macrophage foam cells. Arterioscler Thromb Vasc Biol 19:1891–1898.
Ko DC, Milenkovic L, Beier SM, Manuel H, Buchanan J, Scott MP (2005) Cell-autonomous death of cerebellar Purkinje neurons with autophagy in Niemann-Pick type C disease. PLoS Genet 1:81–95.
Kretzschmar D, Hasan G, Sharma S, Heisenberg M, Benzer S (1997) The swiss cheese mutant causes glial hyperwrapping and brain degeneration in *Drosophila*. J Neurosci 17:7425–7432.
Langmade SJ, Gale SE, Frolov A, Mohri I, Suzuki K, Mellon SH, Walkley SU, Covey DF, Schaffer JE, Ory DS (2006) Pregnane X receptor (PXR) activation: a mechanism for neuroprotection in a mouse model of Niemann-Pick C disease. Proc Natl Acad Sci USA 103:13807–13812.
Lee T, Luo L (1999) Mosaic analysis with a repressible cell marker for studies of gene function in neuronal morphogenesis. Neuron 22:451–461.
Lee T, Lee A, Luo L (1999) Development of the *Drosophila* mushroom bodies: sequential generation of three distinct types of neurons from a neuroblast. Development 126:4065–4076.
Liao G, Yao Y, Liu J, Yu Z, Cheung S, Xie A, Liang X, Bi X (2007) Cholesterol accumulation is associated with lysosomal dysfunction and autophagic stress in npc1−/− mouse brain. Am J Pathol 171:962–975.
Loftus SK, Erickson RP, Walkley SU, Bryant MA, Incao A, Heidenreich RA, Pavan WJ (2002) Rescue of neurodegeneration in Niemann-Pick C mice by a prion-promoter-driven Npc1 cDNA transgene. Hum Mol Genet 11:3107–3114.
Lusa S, Blom TS, Eskelinen EL, Kuismanen E, Mansson JE, Simons K, Ikonen E (2001) Depletion of rafts in late endocytic membranes is controlled by NPC1-dependent recycling of cholesterol to the plasma membrane. J Cell Sci 114:1893–1900.
Millard EE, Gale SE, Dudley N, Zhang J, Schaffer JE, Ory DS (2005) The sterol-sensing domain of the Niemann-Pick C1 (NPC1) protein regulates trafficking of low density lipoprotein cholesterol. J Biol Chem 280:28581–28590.
Min KT, Benzer S (1997) Spongecake and eggroll: two hereditary diseases in *Drosophila* resemble patterns of human brain degeneration. Curr Biol 7:885–888.
Mukherjee S, Maxfield FR (2004) Lipid and cholesterol trafficking in NPC. Biochim Biophys Acta 1685:28–37.
Naureckiene S, Sleat DE, Lackland H, Fensom A, Vanier MT, Wattiaux R, Jadot M, Lobel P (2000) Identification of HE1 as the second gene of Niemann-Pick C disease. Science 290:2298–2301.
Ohgami N, Ko DC, Thomas M, Scott MP, Chang CC, Chang TY (2004) Binding between the Niemann-Pick C1 protein and a photoactivatable cholesterol analog requires a functional sterol-sensing domain. Proc Natl Acad Sci USA 101:12473–12478.
Pacheco CD, Kunkel R, Lieberman AP (2007) Autophagy in Niemann-Pick C disease is dependent upon Beclin-1 and responsive to lipid trafficking defects. Hum Mol Genet 16:1495–1503.
Palladino MJ, Bower JE, Kreber R, Ganetzky B (2003) Neural dysfunction and neurodegeneration in *Drosophila* Na+/K+ ATPase α subunit mutants. J Neurosci 23:1276–1286.
Patel SC, Suresh S, Kumar U, Hu CY, Cooney A, Blanchette-Mackie EJ, Neufeld EB, Patel RC, Brady RO, Patel YC, Pentchev PG, Ong WY (1999) Localization of Niemann-Pick C1 protein in astrocytes: implications for neuronal degeneration in Niemann-Pick type C disease. Proc Natl Acad Sci USA 96:1657–1662.
Paul CA, Boegle AK, Maue RA (2004) Before the loss: neuronal dysfunction in Niemann-Pick Type C disease. Biochim Biophys Acta 1685:63–76.
Reddy JV, Ganley IG, Pfeffer SR (2006) Clues to neuro-degeneration in Niemann-Pick type C disease from global gene expression profiling. PLoS ONE 1:e19.
Reid PC, Sakashita N, Sugii S, Ohno-Iwashita Y, Shimada Y, Hickey WF, Chang TY (2004) A novel cholesterol stain reveals early neuronal cholesterol accumulation in the Niemann-Pick type C1 mouse brain. J Lipid Res 45:582–591.
Rietveld A, Neutz S, Simons K, Eaton S (1999) Association of sterol- and glycosylphosphatidylinositol-linked proteins with Drosophila raft lipid microdomains. J Biol Chem 274:12049–12054.
Rohrbough J, Broadie K (2005) Lipid regulation of the synaptic vesicle cycle. Nat Rev Neurosci 6:139–150.
Rohrbough J, O'Dowd DK, Baines RA, Broadie K (2003) Cellular bases of behavioral plasticity: establishing and modifying synaptic circuits in the *Drosophila* genetic system. J Neurobiol 54:254–271.
Rohrbough J, Rushton E, Palanker L, Woodruff E, Matthies HJ, Acharya U, Acharya JK, Broadie K (2004) Ceramidase regulates synaptic vesicle exocytosis and trafficking. J Neurosci 24:7789–7803.
Sanxaridis PD, Cronin MA, Rawat SS, Waro G, Acharya U, Tsunoda S (2007) Light-induced recruitment of INAD-signaling complexes to detergent-resistant lipid rafts in *Drosophila* photoreceptors. Mol Cell Neurosci 36:36–46.
Schmitz G, Muller G (1991) Structure and function of lamellar bodies, lipid-protein complexes involved in storage and secretion of cellular lipids. J Lipid Res 32:1539–1570.
Scott C, Ioannou YA (2004) The NPC1 protein: structure implies function. Biochim Biophys Acta 1685:8–13.
Scott C, Higgins ME, Davies JP, Ioannou YA (2004) Targeting of NPC1 to late endosomes involves multiple signals, including one residing within the putative sterol-sensing domain. J Biol Chem 279:48214–48223.
Sepp KJ, Schulte J, Auld VJ (2001) Peripheral glia direct axon guidance across the CNS/PNS transition zone. Dev Biol 238:47–63.
Simons K, Gruenberg J (2000) Jamming the endosomal system: lipid rafts and lysosomal storage diseases. Trends Cell Biol 10:459–462.
Sturley SL, Patterson MC, Balch W, Liscum L (2004) The pathophysiology and mechanisms of NP-C disease. Biochim Biophys Acta 1685:83–87.
Thummel CS (1996) Files on steroids–Drosophila metamorphosis and the mechanisms of steroid hormone action. Trends Genet 12:306–310.
Tschape JA, Hammerschmied C, Muhlig-Versen M, Athenstaedt K, Daum G, Kretzschmar D (2002) The neurodegeneration mutant lochrig interferes with cholesterol homeostasis and Appl processing. EMBO J 21:6367–6376.
Tschape JA, Bettencourt da Cruz A, Kretzschmar D (2003) Progressive neurodegeneration in Drosophila: a model system. J Neural Transm Suppl 51–62.
Vance JE (2006) Lipid imbalance in the neurological disorder, Niemann-Pick C disease. FEBS Lett 580:5518–5524.
Vance JE, Karten B, Hayashi H (2006) Lipid dynamics in neurons. Biochem Soc Trans 34:399–403.
Vanier MT, Millat G (2003) Niemann-Pick disease type C. Clin Genet 64:269–281.
Voght SP, Fluegel ML, Andrews LA, Pallanck LJ (2007) Drosophila NPC1b promotes an early step in sterol absorption from the midgut epithelium. Cell Metab 5:195–205.
Walkley SU, Suzuki K (2004) Consequences of NPC1 and NPC2 loss of function in mammalian neurons. Biochim Biophys Acta 1685:48–62.
Wu YP, Mizukami H, Matsuda J, Saito Y, Proia RL, Suzuki K (2005) Apoptosis accompanied by up-regulation of TNF-alpha death pathway genes in the brain of Niemann-Pick type C disease. Mol Genet Metab 84:9–17.
Xie C, Turley SD, Pentchev PG, Dietschy JM (1999) Cholesterol balance and metabolism in mice with loss of function of Niemann-Pick C protein. Am J Physiol 276:E336–E344.
Xie C, Burns DK, Turley SD, Dietschy JM (2000) Cholesterol is sequestered in the brains of mice with Niemann-Pick type C disease but turnover is increased. J Neuropathol Exp Neurol 59:1106–1117.
Yao KM, White K (1994) Neural specificity of elav expression: defining a *Drosophila* promoter for directing expression to the nervous system. J Neurochem 63:41–51.
Zervas M, Somers KL, Thrall MA, Walkley SU (2001) Critical role for glycosphingolipids in Niemann-Pick disease type C. Curr Biol 11:1283–1287.